

# Chapter 6

---

## Efficient Visualization of Dose Distribution

### 6.1 Introduction

Completing the steps of the RTP process described in the previous chapters of this thesis, we enter now into a different area that involves the evaluation of the treatment planning results. As already mentioned, the CT-Simulation of standard treatment cases follows, the calculation of dose distribution for the proposed radiation field arrangement. Recently we pierce a new era in RTP where exchange of planning data among different processing and visualization modalities happens more freely and standardized using DICOM-RT, than never before. In previous chapters we demonstrated graphical tools that can be available during the CT-simulation of the planning process, involving the definition, selection and display of volumes of interest in relation to the neighbor anatomy and radiation beam geometry. These tools are meant to augment the traditional display methods giving physicians and physicists the ability and flexibility to visualize complex information in various formats. The product of the simulation process is forward to the dose calculation engine. For calculating dose distributions the density information is taken from the CT volume. Additional important information for this process is the geometric primitives of the volumes of interest and the radiation beam orientation and shape.

The dosimetric analysis is important in order to choose between a number of apparently radiation beams arrangements and to optimise the weighting of doses from a number of beams in a given arrangement [Peliz96]. By appropriately weighted integrations of calculated doses over the volume of tumour and normal structures segmented from the CT data, dose volume histograms (DVH), estimates of tumour control probability (TCP) and normal tissue complication probabilities can be produced. The group of dose verification tools is completed with additional visual verification in two and three dimensions. The ability to make such calculations relies on the accurate definition of the 3D region of integration and dose volume grid resolution.

It is very common in dose distribution computations, to make a trade-off between performance and accuracy. Due to visualization performance and interactivity issues most RTP systems reduce the dose volume grid, which usually has four to eight times smaller resolution compared with the original CT volume. In any case the aim of dose display is the same: clear illustration of the spatial relationship between the structures of interest and the dose distribution. Commonly this is achieved using a surface representation (polygon or voxel based) of the corresponding objects, selecting among opaque and semi-transparent appearance. To answer the question why surfaces are most suitable for this task, one should consider as remarks that our world is dominated by surfaces. Thus we can better evaluate the shapes and spatial relationships of objects from reflections of their bounding surfaces than from transmission or scattering of light through their interior [LeFuP90].

Most RTP applications distinguish the rendering methods into surface (polygon) rendering and volume rendering methods. Originally 3D RTP systems displayed the surfaces of 3D objects as stacks of contours. The wire-loop visualization conveys the defined important features of the 3D image scene using a minimal amount of on-screen information. These visualization techniques can still be found useful and are widely used [Purdy93], [Perez95], [Peliz98]. The most important advantage of this representation approach is the minimization of the amount of information used to define a 3D structure shape, meaning that the displayed objects may be manipulated at interactive rate without any pre-processing and interpolation step of missing data. The more developed surface rendering displays using polygon models of surfaces have also been heavily used in treatment planning systems. Hardware acceleration to directly render polygon scenes has a long history and currently is available at modest cost e.g. personal computers. To complete the visualization scene all regions of interest, target and critical normal structures, are manually or semi-automatically segmented and geometric models of them are generated. Dose iso-surfaces are automatically extracted from the dose volume into polygon meshes using marching cubes. Wire-loop and surface-based visualizations are effective for displaying geometrically defined objects and have the advantage that all objects involved in the RTP process such as dose iso-surfaces, objects of interest and radiation beam boundaries, can be included in the rendered view, as opaque or semitransparent surfaces and inter-mixed ease using the same graphics techniques.

Despite the above advantages of the wire-loop and surface-based visualizations, they have not proven entirely satisfactory for displaying anatomy and dose. This is part because surface rendering requires that each anatomic featured must be contoured, a time consuming and labour intensive process. The resulting polygonal mesh not only omits potentially useful information, but also creates the false illusion that features have well defined surfaces. For display radiation dose with a smooth mesh a large number of polygons must be used. In order to display different dose levels separated meshes must be generated in the same manner.

Volume rendering is a well-established method in medical imaging for generating high realistic three-dimensional images lack of intermediate contours or polygon meshes. As described in Chapter-5, volume rendering generates images after direct sampling of the volume data values. Voxel classification is often used to assign to each voxel a set of visual attributes, such as colour and intensity. In addition the opacity is commonly used property that measures how much intensity of the sampling ray will pass through a given material. Similarly to the visualization principles of multi-volume rendering methods used in data fusion of different imaging modalities, in RTP the data volumes involved in the process, volumes of interest, CT data and dose volume, are combined under the same graphic environment independent from their resolution [Vanuy99]. Common volume rendering examples are applications in stereotactic treatments [Gehri91], [Peliz98], [VDBer00]. The principal advantage of volume rendering over wire-loop and polygon-based visualization are their superior image quality and the ability to generate images without explicitly defining the geometry of the structures. Even when object geometry must be defined, as it often happens in RTP, using volume rendering one has always the possibility to reconstruct selectively parts of the original volume without significant effort but with significant visual benefits. One approach is to use an auxiliary volume, which will have the same size as the original data volume [Schim93]. The segmented objects will allocate a corresponding amount of voxels in the auxiliary volume addressing their geometrically shape. Then the 3D reconstruction could be achieved using the same rendering

pipeline. A different approach is the use of hybrid rendering where the object's shape is defined as polygons objects. The ability to effectively combine volume and surface graphics has important implications for intra-operative visualization and haptic rendering systems [LeFuP90], [Bhale00], [Seem01].

CT simulation offers high quality 3D images that are mostly used for the planning of the patient treatment. Important influence on producing these results has the high resolution CT volume used. The 3D visualization of all the necessary information combined, can be done interactively, which is of great benefit for the clinical routine. In combination to the above advantages the display of the treatment plan registered with the dose volume information produced from the TPS will further enhance the treatment evaluation process and the role of CT-simulation in the RTP process. In this chapter we will present a visualization strategy that described the dose display process within the CT-simulation environment. The work of this chapter could be separated into two parts: the dose resampling and dose visualization part. The first part involves the interpolation of the original dose volume data; a critical step when aiming to produce accurate calculation results as well as high quality 3D illustrations. The second part involves the mixed visualization between the dose and the CT-volume in two and three dimensions. Volume rendering is the vital component used for the implementation of the visualizations tools that will be presented, and aim to augment the qualitative verification of the dose distribution, the volumes of interest and the CT data.

## 6.2 Related Work

One could assign the simultaneous display of dose and CT volume to the multi volume visualization problem. The information acquired from the multimodality volumes can be combined and presented on 2D or 3D schemes. Volume rendering is probably the most common visualization principle technique employed among the existing visualization methods. Cehring *et al.* [Cehri91] presented a system in the frame of stereotactic RTP. There dose volumes could be merged with CT data and segmented volumes. The basis of this application was volume rendering but nevertheless 2D visualization capabilities such as virtual cutting planes and multiplanar reconstructions where also presented as important tools. Levoy *et al.* [LeFuP90] reported a working frame where multimodal anatomical volumes could be rendered registered with the corresponding dose distribution in the frame of RTP. Zuiderveld in his work [Zuide95] presented complete solution on how to combine different imaging modalities such as CT, MR and SPECT. Pelzzari *et al.* in his report [Peliz98], has been more application oriented reviewed several systems involved in visualization issues on RTP. Most of the reviewed systems used as basis volume rendering for visualizing patient's anatomy and volumes of interest. Cai *et al.* [CaiSa99] used volume-rendering techniques to visualize CT-volume of interests and dose volumes under the same visualization scene, investigating all possible optical models that could be adapted on the frame of this task. The results included visualization models based voxel-surface representation as well as on transparent illumination models. This work provided detailed information on a number of potential methods that could be used in RTP visualization.

The aim of this work is to define and present an imaging strategy employed in the frame of 3D-Simulation that would be able to evaluate the dose volume distribution of the applied treatment plan merged with the CT data and the volumes of interest. Basically our aim is to merge three different volumes:

1. The anatomical volume. This represents the original digital patient data as acquired from the imaging modality (this could be CT or MR volumes).
2. The volumes of interest (VOIs). These involve the representation of anatomical regions such as the tumour and organs at risk, defined manually or automatically from the user during the segmentation step.
3. The dose volume. The dose volume is generated from a dose calculation engine considering the corresponding treatment plan, target volume and organs at risk.

For the sake of understanding we have to make clear that the CT volume is the only digital information produced with direct relation from the patient's anatomy. We could call it as *first level* of information. The volumes of interest have been generated based on the anatomical-geometric information provided from the CT data, and thus they belong to the *second level* of information. Finally the dose volumes are also a product of the second level of information and thus we could address it as *third level* of information. Despite the fact that in each level of information an error might be introduced either systematic or randomised, there could be several combinations of the above information so as to produce the best visual outcome. The following diagram illustrates an overview of all possible volume grouping. One could separate the volume illustration methods into three groups of

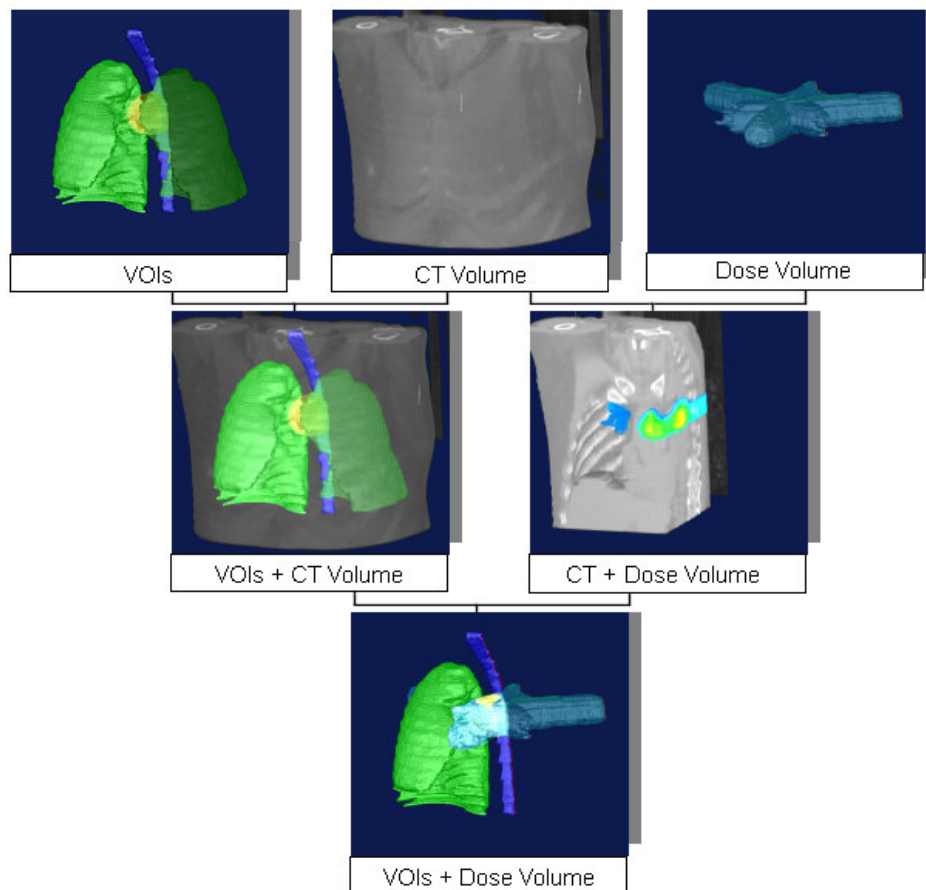


**Figure 6-1.** Selective combination of RTP volumes. The different levels of information are illustrated on the top row; segmented VOIs, CT volume and dose distribution volume. The lower rows indicate different combination possibilities.

information; in the first group of information all volumes are visualized separated from each other. In the second group of information the CT volume is the one who could be combined with the two generate. At this point we have to mention the illustration of the irradiation beams will not provide any additional information when combine with the dose treatment volume.

The way to the final visual outcome must go through several steps such as pre-processing and visualization. A complete approach for the efficient visualization of RTP information should include a range of 2D and 3D tools. In this work we focus in the 3D display of the treatment planning information. The strategy used here involves:

1. **Dose Volume Interpolation:** One problem that often occurs in dose and anatomical volume visualization is the fact that data with different resolutions must be merged. Dose volumes are calculated in a much smaller resolution than the corresponding anatomical volumes (CT or VOIs). Therefore a step is required order to upgrade the dose volume. In this work the interpolation scheme will be applied as a data pre-processing step. Main advantages for that decision is the optimal integration of the interpolated volume to the existing working pipeline, the quantitative and qualitative improvement of the optical result including, the reduction of the processing costs.
2. **Volume Registration:** This step is necessary in order to bring all volumes under the same coordinate system. This can be achieved by applying transformations on the volume geometry.
3. **Visualization:** Visualization aims to merge the CT, VOIs and dose information. The result can be represented in 2D and 3D.

### 6.3 Dose Volume Interpolation

In daily clinical routine the CT devices produce digital data volumes that are composed of 2D slices, with constant resolution  $I_m = (U, V) = (512 \times 512)$ . An average resolution for radiotherapy volumes in 3D-Simulation is  $V = (X, Y, Z) = (512 \times 512 \times 85)$ . However the radiotherapy treatment planning systems, due to their design limitations use much less slices. In addition the patient's CT data are then further converted to a density volume, which has a much lower resolution than the original CT data. The main reason for that is the calculation performance. Finally the generated density volume is feed into the dose calculation engine with the defined anatomical structures and the radiation field configuration. The result of this process is a dose volume that contains missing information when one attempts to combine it with the original CT data volume. Additional reasons to reduce the dose volume during the calculation step but also during the communication (I/O) step is the data visualization. As already discussed, in radiation therapy applications the polygon reconstruction methods are used to illustrate the dose iso-surfaces [Zelez97]. However one can realize the higher the resolution of the dose grid the more demanding are the requirements on memory capacity and processing power during user interaction.

Basically one could use two different approaches to handle missing data. One uncommon approach used in scientific visualization is "by indicating the missing data by mapping colour outside the valid data domain or by making those areas completely transparent" [Twidd94]. However this method would give an abstracting feeling to the clinicians since the presented result is much different from what they have been trained to use as "real". However the most common method used in scientific and medical visualization to

eliminate discarding gaps caused from missing data is interpolation. Interpolation is the process that serves to determine the values of a function at the positions of the missing data, which of course are lying between the original data samples. This is achieved by fitting a continuous function through the discrete input samples [Wolbe90]. The advantage and disadvantage of the interpolation process, usually causes smoothing to the sampled data and do not allow distinguishing the original and interpolated data.

Data interpolation could be separated in two main categories: the scattered data interpolation and the Cartesian grid data interpolation. In the first category belong the interpolation methods that deal with unstructured data that have no special configuration. In contrast the data samples might lie on the vertices of a regular Cartesian grid. The data type used in this work belongs into the second category. For scatter data interpolation literature the reader can refer to [Vasil83], [Books89], [Niels93], [Savch95], [Lee97], [Carr97], [Rohli99], [Carr01], [Morse01], [Turk02].

Regular grid interpolation methods are very often applied in scientific visualization, mostly when at the image reconstruction step aiming to remove aliasing artifacts. An extended literature can be found on the comparison of interpolation schemes over visualization applications. Depending on the application one might use the perceptual approach or the mathematic approach to investigate the interpolation filter performance [Wolbe90], [Mölle97], [Carr98]. In the next paragraphs we will show the impact on the qualitative visualization of the three most common techniques used for the interpolation of regular grid data in scientific visualization, in the frame of RTP. The techniques under investigation will be the nearest neighbour (NN), the tri-linear data interpolation and the BC-Spline interpolation algorithms.

### 6.3.1 Nearest Neighbour (NN)

Nearest neighbour refer to the simplest replacement of missing data and is indeed the simplest interpolation algorithm from the computational point of view. Each interpolated output pixel or voxel is assigned the value of the nearest sample point in the input data. In the spatial domain the NN interpolation can be achieved by convolving the sampling data with a one-sample width rectangle. The interpolation kernel for the NN algorithm is defined as:

$$h(x) = \begin{cases} 1 & \text{when } 0 \leq |x| < 0.5 \\ 0 & \text{when } 0.5 \leq |x| \end{cases} \quad \text{Eq 6. 1}$$

The NN achieves magnification by pixel replication and minimisation by sparse point sampling. The sampling result of the NN algorithm is images with blocky appearance and with potential shift errors of up to 1 ½ pixel-voxels. This approach is inappropriate when sub-sample accuracy is required from the application. Nowadays this interpolation scheme is rarely used in medical application but it is still suitable for real time interactions and data preview. In Figure 6-4 the row (b) illustrates 3D images of two phantom objects reconstruction using the NN interpolation.

### 6.3.2 Linear data interpolation

Assuming a simple 1D example of sampling points linear interpolation offers a first degree connectivity among the sampling points, passing a straight line through every two

consecutive points of the input signal. In the spatial domain, linear interpolation (LN) is equivalent to convolving the sampled data with the following interpolation kernel:

$$h(x) = \begin{cases} 1-|x| & \text{when } 0 \leq |x| < 1 \\ 0 & \text{when } 1 \leq |x| \end{cases} \quad \text{Eq 6. 2}$$

The above interpolation kernel corresponds to a reasonably good low-pass filter in the frequency domain [Wolbe90]. The linear interpolation filter has reasonably superior frequency response compared to the NN filter. Nevertheless, a significant amount of spurious high-frequency components continue to leak into the pass-band, contributing to aliasing. The linear interpolation offers improved interpolation results over NN.

In practice we can define the linear interpolation between two points  $p_0$ ,  $p_1$  in one dimension as follows:

$$p_x = (1-x)p_0 + xp_1 \Rightarrow \quad \text{Eq 6. 3}$$

$$p_x = p_0 + x(p_1 - p_0)$$

The parameter  $x$  represents the fractional position between the data points and has value ranges as defined in Eq 6. 2. In two dimensions the interpolation scheme will involve four data points  $p_{00}$ ,  $p_{01}$ ,  $p_{10}$  and  $p_{11}$ . The interpolation can be formulated using the following formula:

$$p_{xy} = (1-x)(1-y)p_{00} + (1-x)yp_{01} + x(1-y)p_{10} + xyp_{11} \quad \text{Eq 6. 4}$$

This interpolation method is known as *bi-linear* interpolation and is commonly applied on image interpolation e.g. when magnifying raster images. In volumetric data linear interpolation is known as *tri-linear* interpolation and estimates the value of the result voxel considering the neighbourhood of eight (8) voxels. If the data points are defined as  $p_{000}$ ,  $p_{001}$ ,  $p_{011}$ ,  $p_{010}$ ,  $p_{100}$ ,  $p_{110}$ ,  $p_{101}$ , and  $p_{111}$  then the new voxel value  $p_{xyz}$  will be estimated by using the following formula:

$$\begin{aligned} p_{xyz} = & (1-x)(1-y)(1-z) \cdot p_{000} + \\ & x \cdot (1-y)(1-z) \cdot p_{100} + \\ & x \cdot y \cdot (1-z) \cdot p_{110} + \\ & (1-x) \cdot y \cdot (1-z) \cdot p_{010} + \\ & (1-x)(1-y) \cdot z \cdot p_{001} + \\ & x \cdot (1-y) \cdot z \cdot p_{101} + \\ & (1-x) \cdot y \cdot z \cdot p_{011} + \\ & x \cdot y \cdot z \cdot p_{111} + \end{aligned}$$

Eq 6. 5

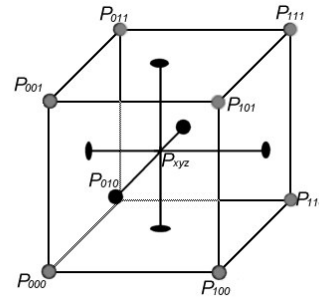


**Figure 6-2.** The geometry of a unit cube with the data points lying on the edges and the interpolated value in position  $(x,y,z)$ .

The parameters  $(x, y, z)$  represent the fractional coordinates of the sampling point  $p_{xyz}$ . The *tri-linear* interpolation is the most common interpolation method used in volume rendering reconstruction and has been realized from several researchers. It is the most widely used interpolation algorithm since it produced reasonably good results at moderate cost. Interpolation result of LN are illustrated in Figure 6-4, row (c).

### 6.3.3 B-Spline Interpolation

Möller *et al.* [Molle97] has investigated the use of cubic spline filters in volume rendering and applied them to MRI data. Their work builds on earlier research by Mitchell *et al.* [Mitch88], which discusses cubic interpolation in computer graphics from a signal processing point of view. They use a Fourier analysis of the approximation error and subjective tests based on 2D image interpolation to argue for a practical cubic spline filter. In [Molle97] a Taylor series expansion is used to argue that the *Catmull-Rom* spline is the optimal interpolator. Interestingly, they choose a different filter, rather than the derivative of the interpolant, to determine gradients. In this paper we have found that, despite these previous analyses, a quasi-interpolant, which does not exactly interpolate the data is useful when rendering structures known to be smooth and continuous. We believe this is because the theoretical analyses do not consider the presence of noise in the sampled data.

By using the cubic B-Spline interpolation we aim to approximate the continuous function, which underlies the volumetric data. The spline control points are therefore derived from the points (voxel centres) where the function is known. In order to apply the B-Spline we will use an approach similar to the parametric representation of curves. If we consider the 1D case the spline interpolation  $S(x)$  specified over the interval  $x_i < x < x_{i+1}$ , can be extracted using the following parametric equation:

Since we refer to 1D by multiplying out the above equation  $S(x)$  can be written as the weighted summation of four points  $P_{i-1}, P_i, P_{i+1}, P_{i+2}$ , which are equally spaced along the interval  $x$ .  $M$  is a  $4 \times 4$  matrix of weights which are chosen to provide various degrees of continuity between adjacent segments at the endpoints  $x=0$  and  $x=1$ . Specifically, we consider the family of BC-Splines where  $M$  is given by:

$$M = \frac{1}{6} \begin{bmatrix} -B-6C & 12-9B-6C & -12+9B+6C & B+6C \\ 3B+12C & -18B+12B+6C & 18-15B-12C & -6C \\ -3B-6C & 0 & 3B+6C & 0 \\ B & 6-2B & B & 0 \end{bmatrix} \quad \text{Eq 6. 7}$$

This family is derived from the most general form for a symmetric cubic basis function. By requiring the value and first derivative to be continuous everywhere, the number of free parameters which determine the spline are the  $(B,C)$ . Note that the BC-Spline family

$$S(x) = X \cdot M \cdot P =$$

$$S(x) = \begin{bmatrix} x^3 & x^2 & x & 1 \end{bmatrix} \cdot \begin{bmatrix} m_{11} & m_{12} & m_{13} & m_{14} \\ m_{21} & m_{22} & m_{23} & m_{24} \\ m_{31} & m_{32} & m_{33} & m_{34} \\ m_{41} & m_{42} & m_{43} & m_{44} \end{bmatrix} \cdot \begin{bmatrix} P_{i-1} \\ P_i \\ P_{i+1} \\ P_{i+2} \end{bmatrix} \quad \text{Eq 6. 6}$$

includes the cubic B-Spline (1,0), the Cardinal cubic Splines (0,C) and the *Catmull-Rom* spline (0,0.5). In this application we select  $(B, C) = (1, 0)$ . Thus matrix M becomes:

$$M = \frac{1}{6} \begin{bmatrix} -1 & 3 & -3 & 1 \\ 3 & -6 & 3 & 0 \\ -3 & 0 & 3 & 0 \\ 1 & 4 & 1 & 0 \end{bmatrix} \quad \text{Eq 6. 8}$$

The properties of the B-spline curves or surfaces can be extended in the image or volume reconstruction very well. The most important properties are continuity, convex hull, local control, variation diminishing and representation of multiple values. The spatial distribution result from B-spline interpolation is smooth and exhibits second order continuity  $C^2$ . The convex hull property of the B-spline ensures that each point in the curve lies in the convex hull of the four control points. Thus, sample points bound the space of the reconstructed curve, surface or volume, so the reconstructed values will range within the voxel values forming the support. The local control property makes far points less influential on the segment of consideration. Thus rapid changes of the control point values in one segment will affect only those point values of the segments lying very near. One method to apply the B-spline interpolation is by estimating the control polygon of the B-spline approximation, such that the resultant case passes through the requested points.

As illustrated in [Foley90] the 1D approach can be extended to 2D as shown below:

$$S(y, x) = [Y \cdot M] \cdot \begin{bmatrix} P_{11} & P_{12} & P_{13} & P_{14} \\ P_{21} & P_{22} & P_{23} & P_{24} \\ P_{31} & P_{32} & P_{33} & P_{34} \\ P_{41} & P_{42} & P_{43} & P_{44} \end{bmatrix} \cdot [M^T \cdot X^T] \quad \text{Eq 6. 9}$$

where:

$$X = [x^3 \quad x^2 \quad x \quad 1]$$

$$Y = [y^3 \quad y^2 \quad y \quad 1]$$

When the product of Eq 6. 9 is evaluated, it can be seen that the B-spline is constrained to lie within the *convex hull* of the four control points, since the coefficients of the four control points range in value between 0 and 1 and sum to 1 for  $0 < x < 1$ .

We now consider the analogous BC-spline in 3D where  $t = (x, y, z)$ . In 3D the control points lie on a regular grid in  $\mathbf{R}^3$  and are denoted by  $P_{i,j,k}$  where  $(i,j,k)$  are integer indices referring to grid locations where the data are known. The nodes of the grid are the voxel centres. The 3D spline is a weighted average of 64 control points in a  $4 \times 4 \times 4$  neighborhood which describes the spatial distribution  $f(x)$  within the volume bound by the eight central voxels (see Figure 6-3). If the locations of these voxels are scaled and shifted such that they lie within the unit cube, then the spline can be formulated as:

$$S(z, y, x) = Z \cdot M \cdot \begin{bmatrix} Y_m & P'_{k-1} & X_m^t \\ Y_m & P'_k & X_m^t \\ Y_m & P'_{k+1} & X_m^t \\ Y_m & P'_{k+2} & X_m^t \end{bmatrix} \quad \text{Eq 6. 10}$$

Where:

$$Z = \begin{bmatrix} z^3 & z^2 & z & 1 \end{bmatrix}$$

$$P'_k = \begin{bmatrix} P_{i-1, j-1, k} & P_{i, j-1, k} & P_{i+1, j-1, k} & P_{i+2, j-1, k} \\ P_{i-1, j, k} & P_{i, j, k} & P_{i+1, j, k} & P_{i+2, j, k} \\ P_{i-1, j+1, k} & P_{i, j+1, k} & P_{i+1, j+1, k} & P_{i+2, j+1, k} \\ P_{i-1, j+2, k} & P_{i, j+2, k} & P_{i+1, j+2, k} & P_{i+2, j+2, k} \end{bmatrix}$$

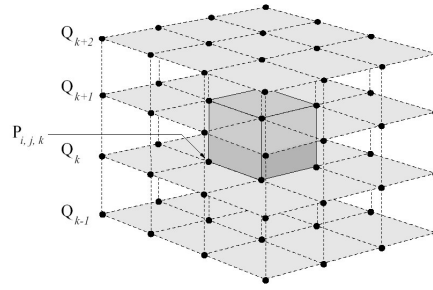


**Figure 6-3.** The geometry of the 64 control points defining the B-Spline in three dimensions.

The aggregate of BC-spline segments determines the scalar distribution over the entire data volume. The resulting spatial distribution is smooth and, in the case of the B-spline, exhibits second order continuity. The convex hull property of the B-Spline means that the fitted function is constrained to have values within the range of the voxel forming the support. Other choices of B and C, such as the *Catmull-Rom* spline, do not exhibit this property. The B-Spline is a *quasi-interpolant* of the voxel values at the interpolation nodes. It is not unreasonable to approximate the sampled data at voxel centers if the sampled data are noisy or do not represent the actual value of the parameter at the grid coordinates but are averages of the true parameter over the volume of the voxel. In such cases, the data can be viewed as having a noise component arising from the partial voluming effect.

In practice, the B-spline interpolant closely approximates the data except where sudden changes occur at a scale, which is small relative to the size of the B-spline support. The piecewise nature of the spline interpolant avoids the propagation of spurious ripples due to sudden changes or discontinuities in the data. Reconstruction examples using different interpolation functions are presented in Figure 6-4. The two phantom data used have original size of  $128^3$  with 1mm square voxel size. For our experiments we have been removing 75% of the original data in regular spaces. Although we expected that the interpolation algorithms would not be able to reconstruct the original object shapes due to the large amount of removed data, we wanted to exam the difference of the reconstructed result with the original shape. We choose that percentage of information reduction due to the fact that several commercial TPS systems that export the dose distribution matrices use a similar ratio for reducing the original data. We use the interpolation algorithms presented above to reconstruct the original shape of the objects. The results indicated that the NN interpolation method reconstructs the original shape with rather deformed edges far from the reality. Linear interpolation improved the situation giving more realistic edges to the original bars. However it has been incapable to reproduce the curvature of the sphere object. Finally the B-Spline has been more efficient on reconstructing the sphere object due the high degree of continuity. However we noticed that shrinkage has been caused to the bar phantom edges, an effect we also observe when interpolating clinical dose distribution data.

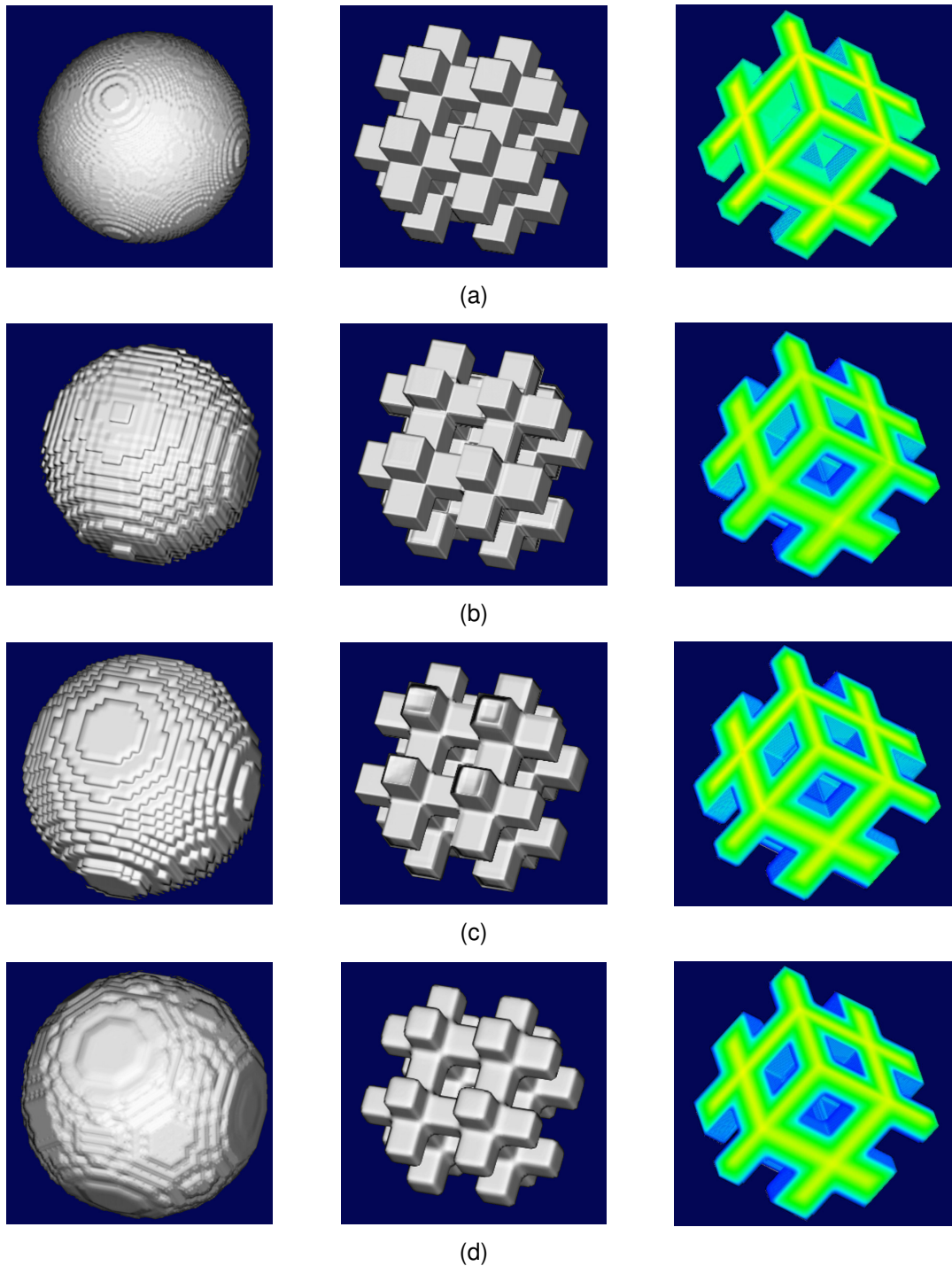


**Figure 6-4.** 3D Reconstruction results of phantom data using different interpolation algorithms. The phantom data have been reduced 75% of the original data volume. From top to bottom (a) represents the original data, (b) the reconstruction after interpolation using the NN, (c) the reconstruction after interpolation using the LN method and (d) the reconstruction after interpolations using B-Spline method.

## 6.4 Dose Volume Visualization

The key component for the volume visualization process is the rendering pipeline. Although the rendering pipeline is already presented in previous chapters, for the sake of integrity we will briefly mention that design again. Rendering algorithm is the ray casting algorithm based on [Sakas93] and [Sakas95]. The main rendering pipeline is similar to the mono-volume rendering pipeline described in [Saka93]. The data flow through three different stages, Geometric Transformation, Integration-in-Depth, and Mapping. In our context, since different volumes share the same size and position, geometric transformation and the mapping are the same as in mono-volume rendering. The difference is in the second stage (see Figure 6-5).

In case that the multi-volumes resolutions are different, the same start and end points in world co-ordinates would relate to different traversing co-ordinates in volume data spaces. In addition, the number of sampling points along the same ray should be different in different volumes due to the different resolutions. In that case simplicity, the largest numbers of sampling points in multi-volumes is used as the number of steps in the ray traversing, which results in an identical loop for all volumes causing over-sampling in the smaller resolution volume. In the context of our work the multi-volumes obtained the same resolution having as reference the volume with the highest resolution. This is one of the advantages having the volume interpolation step at the preprocessing level since the sampling process occurs at the same frequency for the multi-volumes. At each sampling point along the ray, the values from different volumes are obtained by sampling and interpolation in the corresponding volume data spaces. Thus, the first two steps in Integration-in-Depth stage become the parallel copies of the corresponding steps in mono-volume rendering.

Cai *et al* [CaiSa99] demonstrated that the multi-volume information can be combined after the above processing step; the data intermixing may be involved in different steps in the Integration-in-Depth stage: in illumination step, in accumulation step or after accumulation. They are corresponding accordingly to illumination model level intermixing, accumulation level intermixing, and image level intermixing. Different intermixing level results in different rendering pipelines. In the context of this work we are interested on qualifying the performance of the volume data mixing methods so as to achieve the best visual outcome.

As presented in section 6.2, in the volume visualization pipeline we should be able to handle three different data combinations obtaining all possible combinations mentioned above. Once again we must refer on the importance of the surface representation (opaque or semi-transparent) of the dose volume in the rendering scheme. The main reason for adapting this policy is the capability offered from the surface representation to better approximate and justify the dose boundaries within the rendering scheme. An X-ray like volumetric reconstruction could be

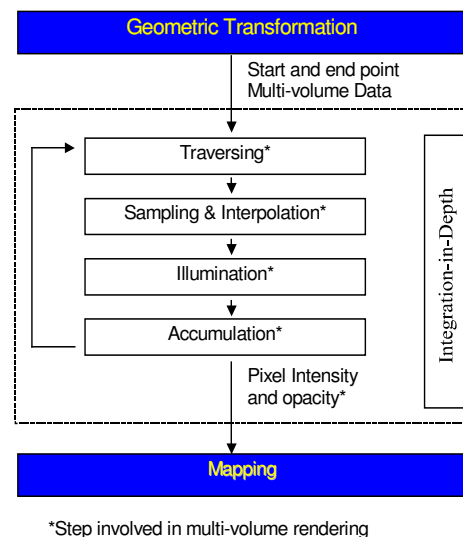


**Figure 6-5.** Simplified diagram of the volume rendering pipeline.

of much less use during dose verification since the accumulated information along the ray and the cloudy appearance of the final result will cause mostly confusion to the observer. Thus in the frame of this work we will use the volumetric surface representation for every volume used.

#### 6.4.1 Merging VOIs and CT Volume

The surface representation of volumetric data has been an old subject in scientific visualization community. Levoy [Levoy88], [LevoA90], [LevoB90] was one of the most successful pioneers in the field presenting the iso-value and gradient representation of volumetric surfaces. The key components of this approach are the calculation of the opacity volume, that has been used to assign transparency properties on the reconstructed surfaces, and the gradient vector estimation that will be used for the shading model as normal vector. The approach employed for this work aims to assign a semitransparent view of the surface of different structures [Höhne90]. In this approach the opacity volume is extracted based on a transfer function (TF) that is generated upon user request similar to the iso-value reconstruction. The TF shape might have a linear or triangular and or higher order of interpolation. During ray traversing and volume sampling a texture value is recorded and filtered with the opacity TF so as to produce an opacity value, lack of gradient vector. Thus the final pixel colour is not affected from any shading model as in the previous case. The interesting affect of this approach is the cloudy appearance of those structures that have been sampled with low opacity values and of course the opaque illustration of the higher opacity values. This approach can be quite useful on illustrating low-density tissues in CT volumes.

The VOIs volume is a product volume of the segmentation process that has been applied on the original CT data. It is very common that the segmented structures are composed of 2D planar contours. There are two common representations used to illustrate a 3D surface from a set of contours. One is to generate a triangulated surface using standard triangulation algorithms. The approach employed in this work is to render-fill the internal region of the contours using a scan conversion algorithm, so as after stacking them to compose a volume that will have the same resolution and size with the original CT data. The filled voxels are addressed with bit values in order to indicate their colour properties and priority properties such as target volume for example. In addition an opacity value is used so as to assign transparency to the segmented objects during the 3D object representation.

An essential part on the shading phase of the binary surfaces is the normal vector on the surface point. There are a number of methods available to estimate normal vectors of discrete surfaces. Usually the normal vector at a surface point is obtained by examining a certain neighbourhood of this point. The methods are denoted as image space or object space techniques, depending on the fact that the neighbourhood is considered in the projected image on in the 3D scene, respectively. Object space techniques are preferred, since they do not suffer from loss of information due to projection. Furthermore, enable rendering techniques like ray tracing, where normal vectors are required in 3D space. The method employed in this work is an object space technique that produces a first estimate of the normal at a surface voxel  $p$  considering a set of voxels in the neighbourhood. For more information on these approaches please refer to [Thürm97], [Thürm01].

The best visual outcome of these two volumes will bring the information about the spatial relation between the segmented structures and the original CT volume. It is important

for the clinical routine to be able to see within the original volume the location of the VOIs. Figure 6-6 shows a single volume reconstruction of the two volumes sampling volumes. The most common method used to merge this different volume information is by blending the two rendering images. For each volume, one result image (intensity and opacity after Integration-in-Depth) is rendered respectively. Then, the final image is calculated by intermixing pixel intensity and opacity coming from the different volumes.

Among the several methods used for image level mixing, the more suitable for the integration of the CT volume and the VOIs, in the content of 3D-Simulation is the use of the following methods:

- Intensity mixing
- Intensity mixing with Z-buffer depth differences.

#### 6.4.1.1 Intensity Intermixing Only

Defining an intermixing factor (or weight)  $w$ , where  $I_1$  and  $I_2$  are intensities coming from two different images, then the result image intensity is the linear composition of two images, i.e.

$$I = w * I_1 + (1.0 - w)I_2 \quad \text{Eq 6. 11}$$

The visual effect of Eq 6. 11 is the fade-in and fade-out of two images when weight is changed interactively. With this effect, user can investigate the relationship of objects in two volumes on a projection plane (see Figure 6-6(c)).

#### 6.4.1.2 Intensity Intermixing with Z-buffer Depth Difference

The main problem of image level intermixing is the lack of correct depth cueing in the overlapping area, where different objects coming from different data set overlap. For example, in Figure 6-6(c), it is difficult to determine the depth location between the two reconstructed structures when they are directly merged with the 3D surface anatomy. For accurate visualization it must be determined, which of these two structures is more near to the viewer. We partially solved the problem using the Z-buffer value<sup>1</sup> of each pixel that represent surface on the image. There are two ways to make use of the Z-buffer depth value. One could be the Z-buffer depth weighting value that could be used during VOIs image generation. The second way is after generating reconstructing the VOI image and the depth values are stored in the Z-buffer. If  $d_{CT}$  and  $d_{VOIs}$  are the depth values in Z-buffer of the two images, then we estimate their depth value difference. The depth difference is normalized and the product is used as the mixing factor between the two images:

$$\begin{aligned} norm\_d &= 1 / \sqrt{(d_{CT})^2 + (d_{VOIs})^2} \\ d'_{CT} &= d_{CT} * norm\_d, \quad d'_{VOIs} = d_{VOIs} * norm\_d \\ w &= w_d * |d'_{CT} - d'_{VOIs}| \\ I &= w * I_{VOIs} + (1.0 - w) * I_{CT} \end{aligned} \quad \text{Eq 6. 12}$$

<sup>1</sup> In volume rendering, the Z-buffer value is defined as the depth along the ray from viewpoint to the first visible voxel of a certain segmented object.

Image level intermixing is very simple and we do not need to change the basic rendering algorithm. Drawback is that the results do not provide the exact correct depth cueing between the two volumes. In Figure 6-6, different mixing factors are used to mix two rendering images, one is CT gradient opacity rendering image, another is segmented object LUT volume rendering image. From left to right, the mixing factor of CT gradient surface image is changed from large to small. Since the mixing of two images is finished interactively, the user can change the mixing factor interactively and viewing the fade-in and the fade-out of two images to smooth over the disadvantage.

## 6.4.2 Merging VOIs and Dose Volume

The accurate dose volume reconstruction is essential for the efficient radiation plan verification. As already mentioned the dose volume has been re-sampled from lower resolution to higher using one of the interpolation methods mentioned above. The highest priority on this visualization step is the common representation of the dose volume in relation with the VOIs. The volumetric surface of the dose has been generated the same reconstruction pipeline used for the VOIs (see Figure 6-8). The colour and opacity properties of the dose volume are assigned means of LUTs (see Figure 6-8). This will allow us to reconstruct different iso-dose levels interactively with different transparencies. For merging the two volumes in this step the image level mixing approach produce poor results since the depth relation of the structures can be misleading. For a better approximation the inclusive opacity intermixing approach is employed. This volume-mixing step is applied during the sampling phase. More precisely within the loop of ray casting, one ray samples voxel values in different volumes at each point and mixes their visual contributions step by step along the ray in accumulation in Integration-in-Depth stage.

The accumulation involves opacity and intensity. Opacity and intensity are derived from the voxel density by a transfer function in the volume illumination model. Since different volumes have different physical background and value ranges, their transfer functions are also different. But opacity and intensity have the same range (between 0.0 and 1.0) and the same optical property after transfer function mapping. Thus, another way is to intermix different opacities and intensities coming from different volumes during the accumulation step. The model used for mixing opacities is based on the inclusive opacity model.

### 6.4.2.1 Inclusive Opacity (INCOP)

Volume mixing using inclusive opacity is a very effective method when using volumes. Furthermore it can be used in surface and volume (surface-voxel) mixing as it has been presented in [Frue91]. Generally speaking, it can be applied in most of the intermixing cases if we can map the voxel value (or any object, like surface and line) into opacity and intensity. Inclusive opacity is to sum up the accumulative effect caused by both opacities from two different volumes and regarding it as the current point opacity. So, the result opacity at the sampling point is,

$$\begin{aligned} \text{opacity} &= 1.0 - (1.0 - \text{opacity}_1) * (1.0 - \text{opacity}_2) \\ &= \text{opacity}_1 + \text{opacity}_2 - \text{opacity}_1 * \text{opacity}_2 \end{aligned} \quad \text{Eq 6. 13}$$

Then, the intensity is,

$$\begin{aligned} I &= \text{norm\_opacity}_1 * I_1 + \text{norm\_opacity}_2 * I_2 \\ \text{norm\_opacity}_i &= \text{opacity}_i / \sum \text{opacity}_n \end{aligned} \quad \text{Eq 6. 14}$$

where  $I$  is the object colour  $I = (R, G, B)$ .

In Eq 6. 14, we use the normalized opacity instead of the original opacity. It means that high opacity voxel has more contribution on the intensity than low one. Although opacity and intensity are mapped from different methods, for example, gradient opacity, iso-value opacity, attenuation opacity, they can be always intermixed by Eq 6. 13 and Eq 6. 14, after mapping them to corresponding opacity and intensity. In Figure 6-8(a) and (b) different dose surface iso-values are reconstructed from the dose volume. The interactive iso-value selection is very useful to view the iso-dose distribution in VOIs. Traditionally, we have to model the iso-surface of dose using polygon surfaces and then mix it into the

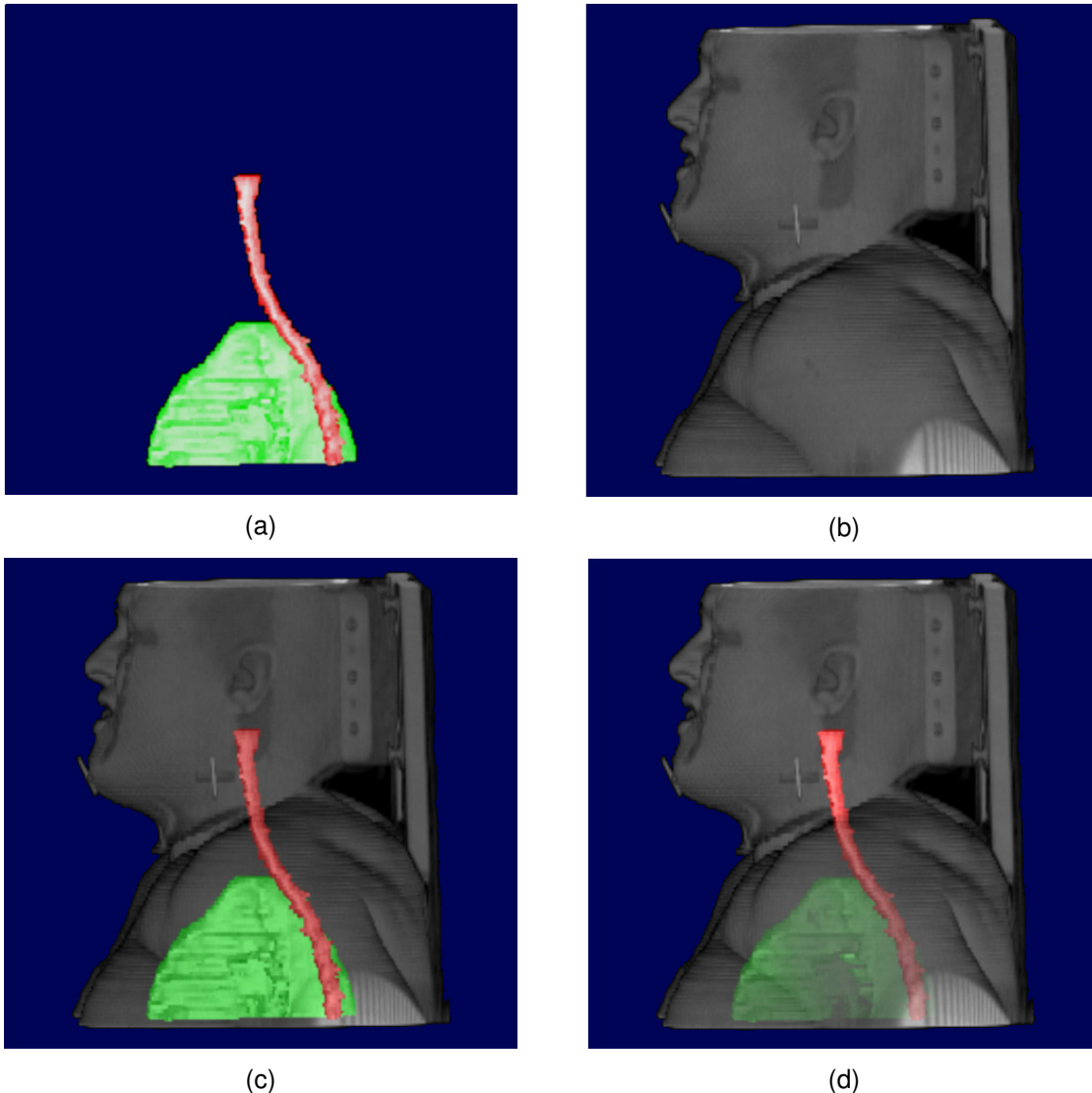


**Figure 6-6.** Volume image mixing using single image intensity blending. In (a) mixing using simple fading effect. In (b) mixing with depth difference weighting.

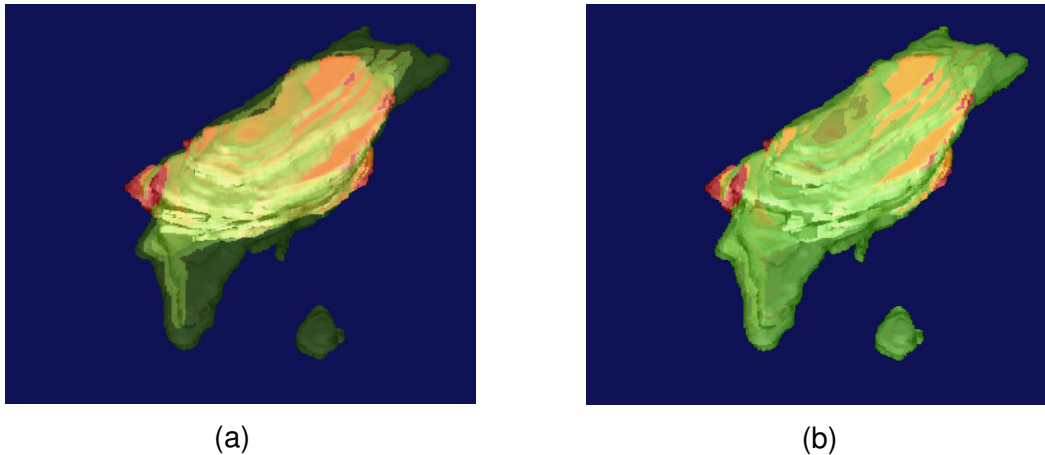


**Figure 6-7.** Target volume and iso-dose volume mixing using the inclusive opacity. From top left to bottom right semi-transparent to opaque reconstruction of the dose volume.

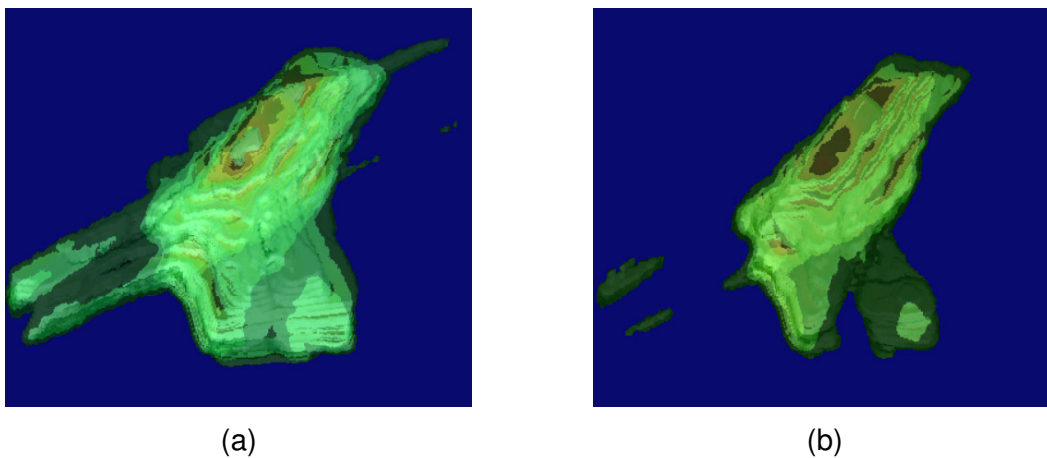


**Figure 6-8.** Iso-value representation of the dose volume. In (a) the selected dose value is lower than the one in (b). In both cases different level of transparencies are used for the corresponding iso-dose values.

anatomy surface structure. Because modeling is a time consuming process and the number of triangles of iso-surface is very large, interactive iso-dose display is almost impossible in iso-surface rendering context.

In Figure 6-7 the segmented volume (in red) is intermixed with the iso-dose volume. The colour and opacity of segmented object is calculated from a lookup table defined by users, while opacity of iso-dose volume is calculated by a function as in [Levo88]. One can observe that iso-dose opacity level can interactively manipulated to provide better geometric relation between the volumes.

#### 6.4.2.2 Dose Mapping on VOIs

The colour mapping process aims to paint the surface of a object with a range of a colour that will refer to the value range of the corresponding metric. These techniques are very commonly employed to other sciences like satellite picture analyses and geographic map

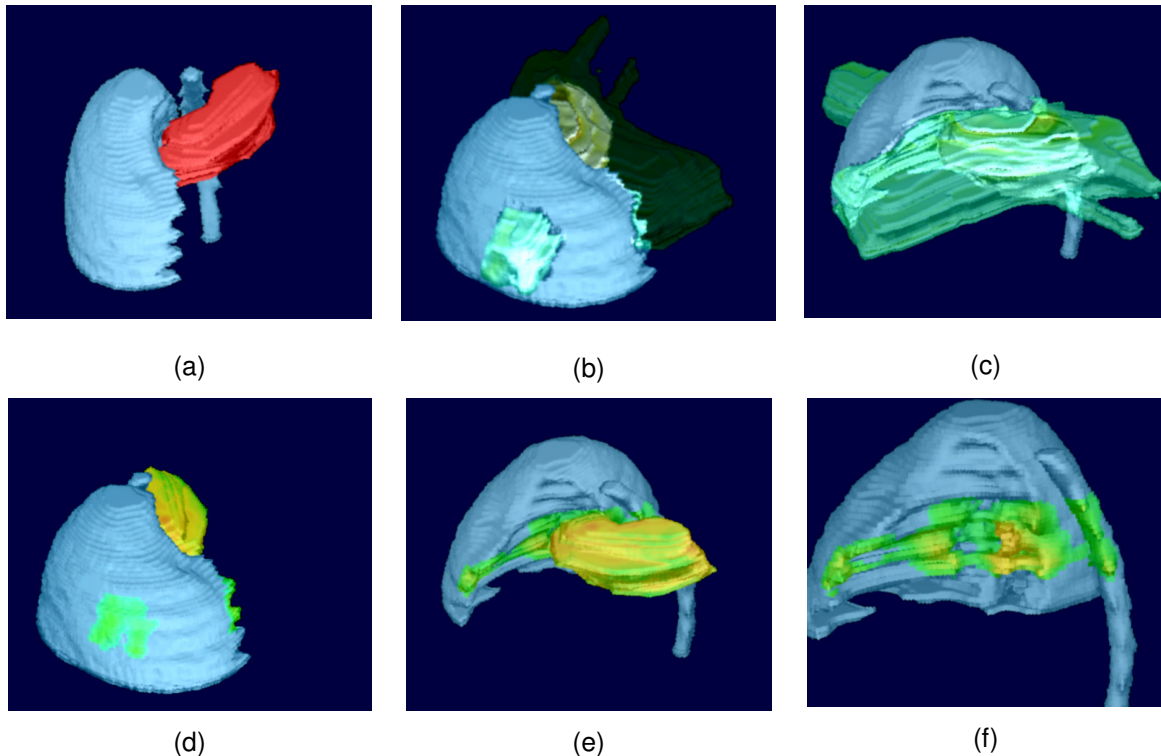


**Figure 6-9.** The effect of dose mapping on VOI surfaces. In (b) and (c) merging of VOIs and dose volumes. In (d), (e) and (f) illustration of cold and hot spots on the surface of the VOI and target volume.

representation. This technique is often used as an evaluation visualization tool that can enhance the value spread of a metric over the geometry of a second metric which is usually considered the one with the priority privileges in the scheme under visualization. In our application we aim to map the dose volume over the VOIs surface, which are our priority volume. This approach could provide an overview of the exposed surface of the VOIs on different dose levels.

The volume mapping can be achieved based on the surfaces depth information collected from the Z-buffer. This means that if surface positions exist for the VOI and at the same time the dose volume intersects that surface then the colour of the VOI surface can be replaced with the colour of the dose volume. In that case the colour value will be combined with the surface normal and the opacity value as calculated from the VOI surface. Basically the rendering pipeline must be modified on the colour accumulation level.

The dose mapping approach is a low cost processing action with very interesting optical results. Figure 6-9 illustrates a semi-transparent representation of the dose volume mixed with the VOIs. The right lung and spine (blue-grey structures) are exposed to the maximum allowed dose levels. The question is what is that level of exposure and where. The level of exposure can be verified using the dose volume histogram approach. However there is still the question of where this exposure takes place. The semi-transparent or the opaque view of the dose volume provides the user with limited information about the exact borders of the exposed region (b). This problem can be solved using the dose mapping approach. In Figure 6-9 (b) one can clearly see the region of the organ exposed

and also the level of the dose. The minimum dose level is defined from the selected iso-dose value. Although the dose mapping effect provides an overview of the dose distribution spread on the segmented volume surface no information are present about the dose distribution depth within the organ volume.

### 6.4.2.3 3D Visualization of the DVH

The term histogram is commonly used in image processing. The image histogram is used as information tool to provide a general description of the image contrast appearance. In a similar manner the dose volume histogram (DVH) provide a description of the radiation dose distribution over the VOIs and can graphically summarize large amounts of 3-D dose distribution information throughout the volume of the tumour or a normal anatomical structure [Drzym91]. The dose volume histogram curve is calculated for each volume of interest by performing a 3D analysis of the dose distribution within a segmented volume. This analysis involves the reappearance of each dose percentage within the volume under investigation. The DVH for a particular dose level  $D_i$  can be defined as:

$$DVH(D_i) = \left( Vol * \sum_{j=1}^{N_D} \delta_j \right) / N_D \quad \text{Eq 6.15}$$

Where  $\delta_j = 0$  if  $D_j < D_i$  and  $\delta_j = 1$  if  $D_j > D_i$ , and  $N_D$  the number of dose points within the volume of the VOI and  $Vol$  the total volume of the organ of interest.

For example if a dose level covers the complete organ volume then this dose level is marked with 100 % (see Figure 6-10). The DVH is probably the most regular tool for treatment plan evaluation and is proven that summarizes large volumes of dose-distribution data to allow rapid screening of rival plans. However the information provided by DVH graph are limited in two ways:

- a. DVHs do not provide spatial information, such as the location of the high- and low-dose regions inside the VOI. In addition no information are provided for the actual organ volume and length under study.
- b. There are algorithms that do not study the dose distribution relation of the organ volume within the treatment field. Instead the complete organ volume is used. This means that large organ volume will give low-risk DVH curve and vice versa.

Considering the above situations the information provided to the user by the DVH might be limited or wrong since it is never clear which part of the structures and the sizes receiving the dose distributions. Several authors worked in the direction of improving the quality and the amount of the DVH information. Niemerko et al. [Niemi94] developed the concept of dose-volume distribution (DVD) and the corresponding differential dose-volume distribution (dDVD) for treatment-plan evaluation. The dose-volume information inherent in the calculation points is used in the calculation of DVDs and dDVDs. An additional variant of the DVH the dose-surface histogram (DSH) [LuY95] and dose-wall histograms (DWH) [Meije99], have been proposed as a treatment-planning tool for hollow structures in prostate conformal therapy. For this walled hollow structures, such as the rectum and the bladder, estimation of the dose-surface is more biologically relevant than the dose to the volume. DVH estimation related with the spatial information of the dose distribution and the VOI information is presented by [Chee99]. Their concept is called the

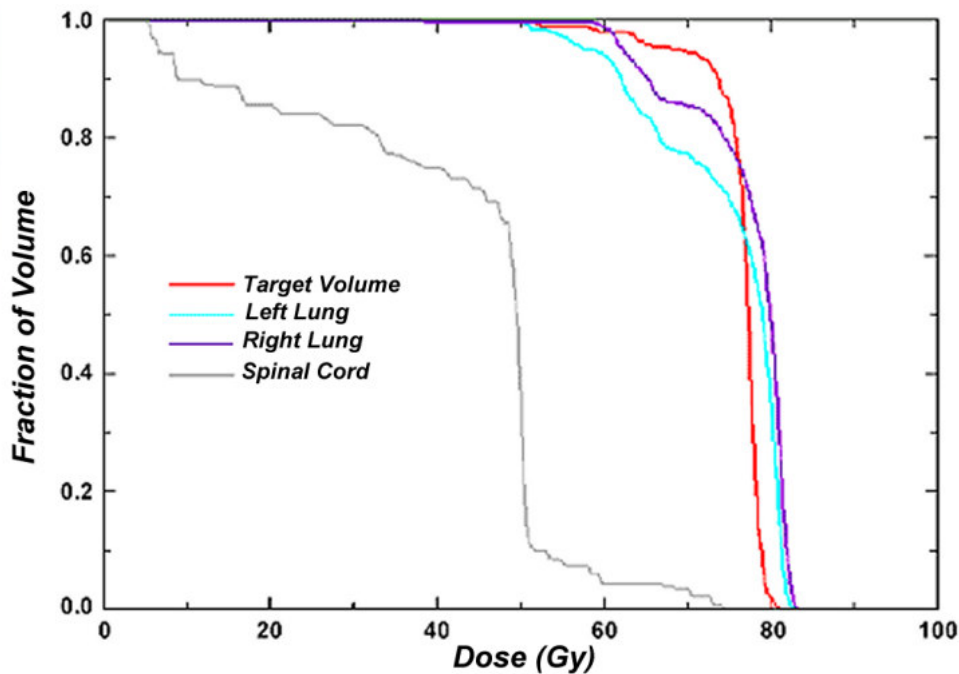


**Figure 6-10.** Illustration of a DVH over four different structures. One can have an overall appreciation of the dose distribution on the different organs. However any conclusion about the treatment is difficult to be taken because due to the lack of spatial information.

z-dependent dose-volume histogram (zDVH) and provides the spatial variation, as well as the size and magnitude of the different dose regions within the region of interest. Thus although DVH provides an average dose-volume information, zDVH provides differential dose-volume information with respect to the CT slice position.

An additional approach related with the DVH and the visualization of the dose distribution is presented in [Kessl94]. Their technique is presented for overcoming a major deficiency of histogram analysis in radiotherapy treatment planning which is the lack of spatial information. In their technique, histogram data and anatomic images are displayed in a side-by-side fashion. The histogram curve is used as a guide to interactively probe the nature of the corresponding 3-D dose distribution. Regions of dose that contribute to a specific dose bin or range of bins are interactively highlighted on the anatomic display, applied to 2D and 3D views as a window-style cursor is positioned along the dose-axis of the histogram display.

In this work we provide a unique graphical solution to that problem, aiming to create a 3D representation of the DVH. To achieve this we have to consider the definition of the DVH. What we are interested is to illustrate the dose distribution over the normal structures exclusively. This means that the rest of the dose volume must be excluded from the reconstruction scene in order to reduce the complexity of the view. When one uses voxel representation for the dose and the segmented organs can apply very easy this explicit operation during the ray traversing process at the sampling step  $i$  :

$$\text{Voxel}_{\text{Dose}}(C_i, O_i) = \begin{cases} \text{voxel}_{\text{Dose}}(C_i, O_i); & \text{if } \text{voxel}_{\text{VOIs}}(C_i, O_i) \neq 0 \\ 0; & \text{else} \end{cases} \quad \text{Eq 6. 16}$$

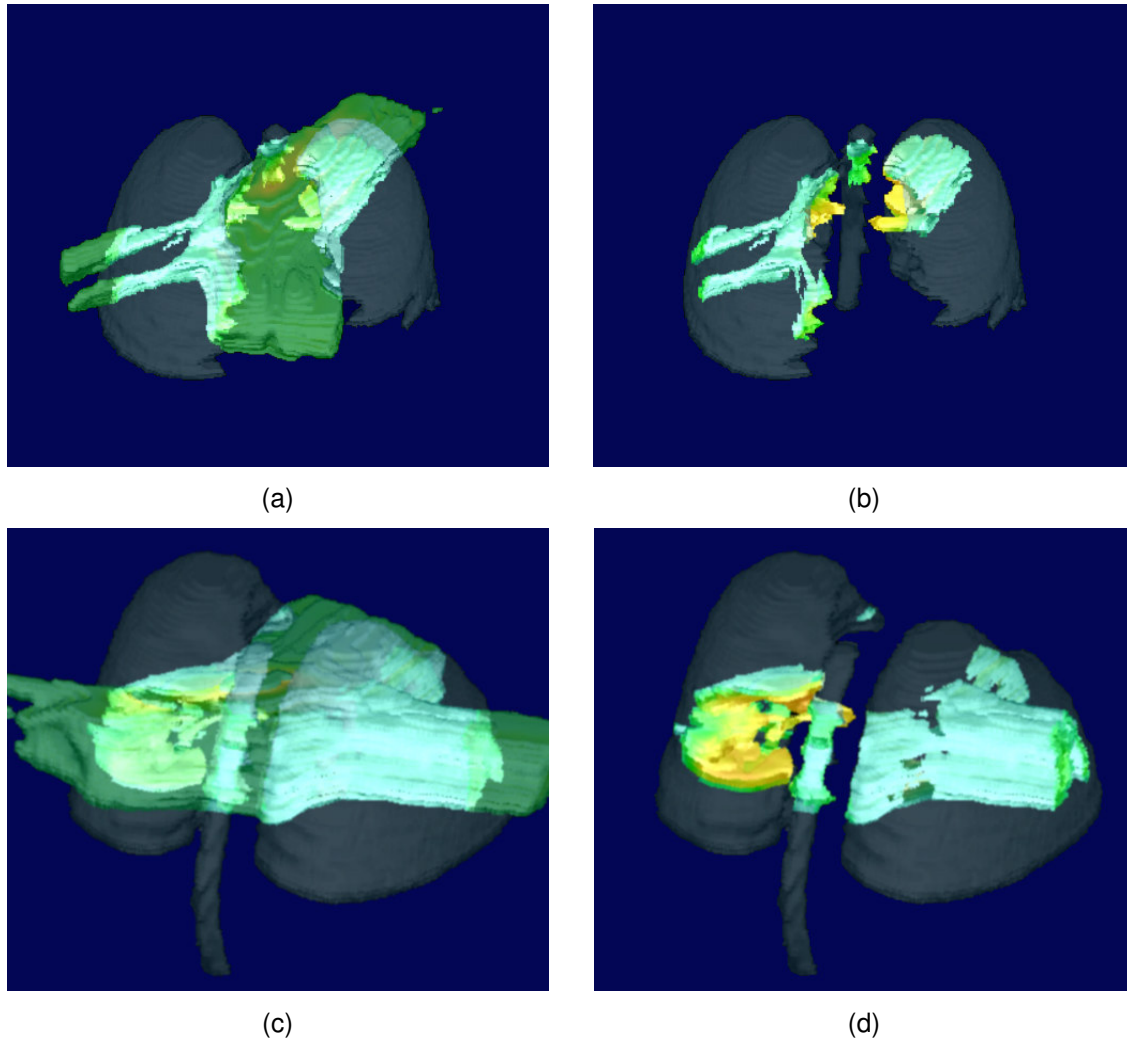


**Figure 6-11.** 3D representation of the DVH. On the left side mixture of the dose volume and segmented organs volume. On the right side the dose volume is reconstructed isolated in the organ volume.

The result of using the Eq 6. 16 will be the isolation of the dose volume within the segmented structure while performing the ray traversing. The next step we have to take is to illustrate the dose distribution within the internal of the structure. This assumes of course that the VOIs are transparent and we illustrate their internal. The volume mixing principle used here is the inclusive opacity. Critical locations for the reconstruction quality of the dose distribution remain the border of the VOI objects where the exclusivity rule is applied on the dose volume. At those locations the calculation of normal is crucial in order to provide smooth results. Basically we have to deal with two different occasions when estimating the normal or gradient estimation of the dose volume in this specific case:

- Dose volume grid that is included inside the VOI. Here the normal estimation will be done considering only the dose volume.
- Dose volume at the borders of the VOIs. Here the normal estimation will be done according to the voxels distribution of VOIs.

As in the previous reconstruction schemes also here the user can set interactively the level of the dose distribution under investigation.

The results of this approach are presented in Figure 6-11. In all reconstructed images the organs have been reconstructed with transparent surfaces and having the same colour among them. The images reconstructed with the standard INCOP approach (a and c) provide a more confusing visual result than the 3D DVH images (b and d). The reason is that several transparent object are involved in the same visual scene causing loss of the accurate depth information of the surfaces. As a result the observer's eye is obstructed from the main focus, which is the dose distribution inside the organ volume. When the dose volume isolation step is applied from Eq 6.15 the result is much more clear and one can notice the differences between the two approaches. This visual effect can be a superior qualitative tool for the dose distribution verification compared to the standard DVH method. The approach can be extremely useful for the verification of the spinal cord exposure on radiation dose. The reason is that the spinal cord is high-risk organ and the maximum allowed levels of exposure are also related with the spine length. The 3D reconstruction of the DVH demonstrates very clear the exposed volume and length of the spine.

### 6.4.3 Merging CT Volume and Dose Volume

In previous sections of this work we demonstrate the visual results when mixing the dose volume and the geometrically defined structures. This mixing approach is the most important graphical verification tool since the view of the segmented objects (VOIs) is enhanced and better appreciated in relation to the dose volume. The geometric definition of the anatomical structures is necessary for visualization and calculation purposes e.g. DVH and is done selectively by the user manually. However in several instances it may be sufficiently to appreciate the relation of the dose volume boundaries to the surrounding organs. In order to avoid the tedious manual organ segmentation process to generate anatomy model of the organ we could use the texture-based volume reconstruction of the anatomical data mixed directly with the dose volume. The reconstruction methods proposed for this task could involve the following alternatives:

- a. direct dose mapping
- b. selective and inclusive opacity

#### 6.4.3.1 Direct dose mapping

In this approach we use the similar principle as in the dose volume mapping on the segmented organs. The ray sampling process accumulates the colour (texture) and the opacity values. If the opacity value has reached the maximum level, which is 1.0 then the accumulation process will be terminated and the corresponding colour  $C_{CT}$  and opacity  $op_{CT}$  value will be exported for the final pixel value  $C_{out}$  calculation Eq 6. 17. At this step, where the ray reached an opaque surface, the dose colour  $C_{Dose}$  value will be sampled if there is any. This colour value will be mixed with the texture colour value to create the final pixel colour using the linear intensity composition of the two colour:

$$C_{out} = \begin{cases} C_{Dose} * w + (1.0 - w) * C_{CT}; & \text{if } voxel_{Dose} \neq 0 \\ C_{CT} * opacity_{CT}; & \text{else} \end{cases} \quad \text{Eq 6. 17}$$

The result of this approach can be seen in the Figure 6-12 and illustrate the dose mapping on the surface of the CT data surface. One can observe the locations where CT opacity is 0 no dose colour is assigned. In addition at locations where the surface is cloudy it is rather uncertain where to assign the dose mapping resulting into unclear visual results. However this method could be ideal when organ surfaces are clearly reconstructed and one wants to verify the level of dose exposure on the structure.

#### 6.4.3.2 Selective and Inclusive Opacity

The second method employed in this work involves volume-mixing approach based on the inclusive opacity approach with a small variation; the opacity sampled from the CT data have higher priority than the dose opacity. Thus in case that no CT opacity is found no accumulation step will occur for the dose volume sampling. However if the CT opacity exists the voxel intensity value will be sampled considering the inclusive opacity. The method improves the visual result of the volume mixing in comparison to the direct dose mapping. The dose volume surface relation with the CT volume can be better appreciated and the intensity variations of the dose volume have smoother transitions since the volume continuity during reconstruction is preserved when CT opacity exists. In anatomical regions with low or zero opacity are dose volume will not be illustrated at all. This effect could be considered as positive if the observer is concentrated on the dose distribution on the opaque structures ignoring the less opaque giving a more clearly image. On the selective opacity approach could lead to wrong decision results since big regions of the dose volumes are not visualized. To overcome this problem we sample both volumes using the standard inclusive opacity model where the complete dose volume will be reconstructed. The results of both approaches are presented in Figure 6-12.

### 6.5 Summary

Evaluating dose volume distribution information in the frame of a 3D-Simulation system is a new concept in the field of RTP. To achieve that a multi-volume methodology is required that will be able to handle several grid data volumes such as CT, segmented organs and dose distribution. First task is to register the different volumes and resample them to the highest resolution available. This step can take place as a pre-processing step using different interpolation algorithms. In this chapter common interpolation methods have been compared using different phantom data. The NN approach is rather inaccurate but fast. Although not reported it can be found even today in commercial radiotherapy applications. The interpolation results shown that LN interpolation can be suitable for the dose data interpolation. In practice most commercial system use this approach for illustrating dose distribution in 2D and 3D. More attractive and smoother results can be achieved using the B-Spline interpolation.

The second part of this chapter involves the visualization of dose information. Among several ways for visualizing dose volumes with medical data, volume rendering has been selected. Since volume rendering is the heart of a 3D-Simulation system we consider this solution closer to our architecture and demands. Thus a voxel-based approach could lead to the smooth integration of this visualization capability within a 3D-Simulation system or more general into a volume visualization package. In addition original CT information can

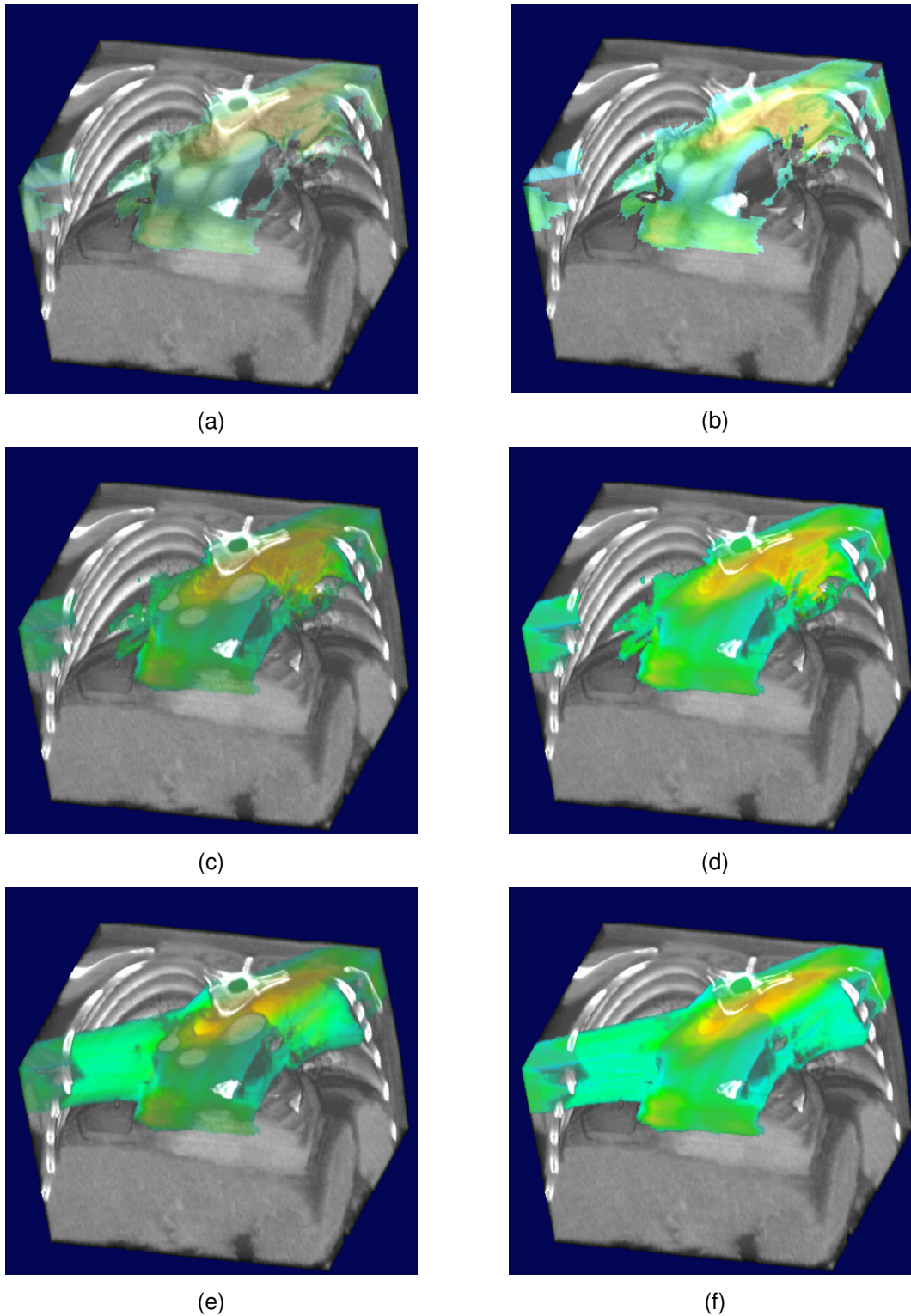


**Figure 6-12.** Merging of CT and Dose volume. The first row (a, b) presents results based on the direct mapping of the dose values on the CT surface. On the second row (c, d) illustration of the CT and dose volumes using selective opacity with priority on the CT volume. On the last row (e, f) the two volumes are mixed including both their opacities.

be visualized at any step and combined with the dose volume creating images that represented effectively the clinical reality.

Here we presented various ways for visualizing of the dose volume information. Scope was to present efficient qualitative dose evaluation tools. Among others unique images are presented that can assist clinicians interpret the DVH information spatially with direct visual comparison of the VOIs. By integrating displays of 3-D doses and the corresponding histogram data, it is possible to recover the positional information inherently lost in the calculation of a histogram. Important questions such as the size and location of hot spots in normal tissues and cold spots within target volumes can be more easily uncovered, making the iterative improvement of treatment plans more efficient.

# Chapter 7

---

## Summary

3D-Simulation comprises two important key words, which recently have often been used to describe a technique for planning the application of radiotherapy without using conventional or in the absence of the actual patient. As an alternative to patient and X-ray simulator, 3D-Simulation uses 3D data set and a series of software tools for accurate planning and re-positioning of the patient. In this work we presented a number of tools of the accurate definition and localization of the tumor volume and further more the evaluation of treatment data and parameters. This chapter provides a summary of the contribution of this thesis in the field of 3D-Simulation. Several algorithms presented here, have been also integrated into 3D-Sim *Exomio*. The clinical relevance and impact of *Exomio* in the treatment of different patient cancer cases can be found in [Zambo02], [Houst02], [Karan02], [Dicks03], [Stras04], [StraV04].

### 7.1 Segmentation of Anatomical Structures

Segmentation is the process that separates an image into its important features (primitives) so that each of them can be addressed separately. This converts the planar pixel of the image into a distinguishable number of individual organs or tumour that can be clearly identified and manipulated. The segmentation process might involve complicate structures and in this case usually only an expert can perform the task of the identification manually on a slice-by-slice base. Humans can perform this task using complex analysis of shape, intensity, position, texture, and proximity to surrounding structures.

In **Chapter 3**, we discussed a daily clinical problem in the frame of 3D simulation and RTP; the accurate definition of anatomical structures in CT data. We present a number of computer-based tools that can assist the segmentation process during the 3D simulation process. The methods presented here are categorized to manual and semi-automatic methods. For the manual volume definition, we present a 3D interpolation method based on implicit functions. Due to the high order of continuity of the function, the interpolation scheme can reconstruct a surface from 3D sample points that describes very accurately several anatomical structures. The input samples can be at the form of parallel contours usually a product of contours defined on parallel imaging cross sections. Even more advanced is the capability of the algorithm to handle the non-parallel contours either perpendicular or even arbitrary placed relative to each other. This has been a new concept for radiotherapy imaging applications.

The conventional 2D segmentation tools on the axial cross sections have been for many years now the standard methods used. Advantages of the new concept is the flexibility and freedom given to the clinicians to investigate new ways of defining anatomical structures taking advantage of the full 3D information available on the multiplanar reconstructed slices such as sagittal and coronal, As a result the segmentation process improves in terms of accuracy. In addition, the time needed to segment structures can be

dramatically reduced since fewer contours are required to describe the shape of the structures.

We demonstrate that segmentation of the spine can be achieved very accurately, in a few seconds with minimum user interaction; the user needs only to define an initial starting point for the algorithm. The algorithm can automatically trace the spine path through the complete volume of cross sections. False contours that do not correspond to the spine shape and position can be rejected automatically from the system and can be replaced with linear interpolated contours considering as key contours those already found by the system. The boundary-tracking methods used belong to the deterministic approaches and therefore there is a tendency to produce misleading results under some circumstances. To reduce that effect data pre-processing and the gradient volume of the original CT data can be used as input to the segmentation routine.

## 7.2 Fast Smoothing of Superficial Respiration Artifacts in CT-Volumes

During CT data acquisition the normal breathing process, internal organ movements, and patient global movements might introduce motion artifacts in the acquired raw data. This motion may be in three dimensions and generally result in artifacts that appear as streaks or distorted semi-transparent structures in the general vicinity of the motion. During tumour irradiation the patient might be immobilized but the breathing process continues normally and freely. In diagnostic imaging it is required from the patient to stop breathing during acquisition to optimise image quality. However the irradiation process lasts more than one minute and therefore it is not possible for the patient to stop breathing. Considering the above it would be more accurate for a CT data acquisition that will be used for the RT planning to record most of organ movements that occur during normal patient conditions. The result of this acquisition will provide with useful information about the movements of specific organs that might be located near or attached to a tumour, and vice versa. This information could assist the more precise assignment of the field size and orientation that will be used to treat the tumour.

Our main interest in the work of **Chapter 4** reflects on the surface movements of the patient. Principally the surface of the patient can be visualized in 3D using voxel or polygon based techniques. Usually the polygon-based techniques are used since the body contours can be defined and modified if necessary from the user. Then triangulation techniques are used to generate a mesh out of the final planar contours. Based on the mesh surfaces several calculations can be performed accurately. In addition to communicate the body contour coordinates between different software systems in the radiotherapy department, the planar contour representation is used as standard geometric format. In radiotherapy it is a common understanding that inaccuracies on patient's body planar contours will lead to inaccurate calculations and analysis related to the patient's body surface since the planar contours are used for reconstructing the patient's surface model.

In **Chapter 4** a dedicated approach is presented for the compensation of the respiratory artifacts on medical body surfaces reconstructed from planar contours. The method can handle fast and efficiently several types of surfaces with respiratory artifacts that might include constant or arbitrary respiration frequencies. The user can define manually constraints on the angular or on the slice level. So far we cannot estimate how the proposed method will influence the results on the clinical environment. This is one part of our future work. In addition we investigate the development of a deformation model that will also compensate the movements of internal structures that deform during respiration.

### 7.3 Improved Volume Rendering of Thoracic CT-Volumes

In many radiation treatment-planning instances, a geometric model of a given anatomical structure is not necessary. Common examples are patients that will receive palliative treatment where no target volume is required. Patients with Hodgkin's disease are mostly treated with two mantle fields, typically from anterior to posterior direction (AP) and posterior to anterior (PA) isocentric beams. The field size and block beam apertures are designed directly on the DRR lack of and target volume and organ at risk. Similarly for patients with breast cancer, during whole breast treatment irradiation, the radiation field arrangement is performed based on the BEV. For the physician it is usually sufficient simply to appreciate the relationship of a target volume to surrounding normal organs. This might involve the visualization of the occlusion of several structures when viewed from a particular perspective. When the volume viewed from the BEV, perspective view, then the user can assess the potentially irradiated structures enclosed in the irradiation field superimposed. The alternative is to use the OEV, orthogonal reconstruction, where the radiation fields reconstructed as opaque or semitransparent polygons are projected with the original CT volume. An additional verification tool can be the use of the virtual light field that presents the intersection of the beam volume with treatment volume

Lungs and trachea belong to the category of the most important organs in the neck and thoracic region. Lung tissue is the one of the dose-limiting structures and it can be exposed in during irradiation of breast tumour, malignant lymphoma and intrathoracic tumours. On the other hand trachea is very often used as organ for orientating the physician during treatment planning of chest and neck tumours. Thus there is a vital importance on visualizing these structures in 3D in relation to neighbour anatomical volumes of the neck and chest region.

In **Chapter 5** we presented the utility of volume rendering reconstruction in the frame of the CT based 3D simulator of radiotherapy planning, focusing on the chest region. Volumetric surface representation of the critical organs in the above region, such as trachea and lungs, are essential to use as anatomical reference markers and to protect respectively. The mentioned anatomical structures must appear with optimum visibility on the reconstructed DRR along the complete 3D simulation process. The proposed method can be integrated in to the main rendering pipeline and requires minimum user interaction for adjusting the necessary parameters. Taking advantage of the volume rendering techniques that offer high quality visualization, we dramatically reduce user effort required for the segmentation of those anatomical structures.

One of the important components of our approach is the use of a binary volume map in order to address all voxels that belong to the air volume that surrounds the patient's body. This processing step is initialised and completed automatically at the data pre-processing level. Then air volume map is used during ray traversing to reject or accept the sampling voxels. The method can improve the visualization of the lungs and trachea surfaces compared to those reconstructed from planar contours. Also, the method can improve the reconstruction of the DRR enhancing the contrast of the subject structures making them applicable for clinical use. Finally by merging both visual information mentioned above we can produce unique images for clinical purpose extending the capabilities of the 3D simulation process and improving treatment planning outcome.

## 7.4 Efficient Treatment Dose Visualization in CT-Simulation

The dosimetric analysis is important in order to choose between a number of apparently radiation beams arrangements and to optimise the weighting of doses from a number of beams in a given arrangement. By appropriately weighted integrations of calculated doses over the volume of tumor and normal structures segmented from the CT data, dose volume histograms (DVH), estimates of tumor control probability (TCP) and normal tissue complication probabilities can be produced. The group of dose verification tools is completed with additional visual verification in two and three dimensions. The ability to make such calculations relies on the accurate definition of the 3D region of integration and dose volume grid resolution. Since the concept of CT simulation focus to reach physicians the qualitative evaluation of dose distribution is essential.

CT simulation offers high quality 3D images that are mostly used for the planning of the patient treatment. Important influence on producing these results has the high resolution CT volume used. The 3D visualization of all the necessary information combined, can be done interactively, which is of great benefit for the clinical routine. In combination to the above advantages the display of the treatment plan registered with the dose volume information produced from the TPS will further enhance the treatment verification process and the role of CT-simulation in the RTP process. In this chapter we will present a visualization workflow that described the complete dose display process within the CT-simulation environment.

**Chapter 6** could be separated into two main parts: the dose resampling and dose visualization part. The first part involves the interpolation of the original dose volume data; a critical step when aiming to produce accurate calculation results as well as high quality 3D illustrations. The second part involves the mixed visualization between the dose and the CT-volume in two and three dimensions. Volume rendering is the vital component used for the implementation of the visualizations tools that will be presented, and aim to augment the qualitative verification of the dose distribution, the volumes of interest and the CT data.

Among several ways for visualizing dose volumes with medical data, volume rendering has been selected, which for our application is the heart of the 3D-Simulation system. Thus a voxel-based approach could lead to the smooth integration of this visualization capability within a CT-simulation system or more general into a volume visualization package. In addition original CT information can be visualized at any step and combined with the dose volume creating images that represented effectively the clinical reality. By integrating displays of 3-D doses and the corresponding histogram data, it is possible to recover the positional information inherently lost in the calculation of a histogram. As shown by the results qualitative display of information can answer important questions such as the size and location of hot spots in normal tissues and cold spots within target volumes. This concept makes the iterative improvement of treatment plans more efficient

## 7.5 Future Directions

Future directions of this work involve the continuation of part of the work done here as well as the investigation of new research directions in the frame of RTP. Future activities will involve:

**Volume Segmentation:** Volume segmentation is an issue where researchers invested many years of efforts. Until today, impressive results have been achieved on segmenting volumes in different application, but no global solution has been adapted, like for example in volume rendering. Radiation therapy is indeed a very demanding era in volume segmentation and definition. The reason for that can be the inconsistency of the CT acquisitions, as well as the variations of patient anatomy due to the disease or patient and organ movements. We believe that the need of further improved manual segmentation tools that can be applied at any image plane will be useful for several occasions in RTP. In addition easy-to-use editing tools can be of great importance. Further more efficient automatic tools can improve the segmentation performance of normal structures. However we believe that this can be achieved up to a number of organs and great influence to that will be the image quality of the imaging modalities.

**Visualization Tools:** Volume visualization is and will continue to be for long time the standards for 3D-Simulation and RTP. Verification procedures, like comparison of electronic portal images with the DRR, require the extraction of anatomical marks or regions from the 2D or 3D data. On this step volume rendering and 2D image processing could be involved. Further more the comparison of multiple dose trials is an essential component for completing the treatment plan evaluation step. We believe that volume rendering can provide interesting results towards this direction.

**Treatment Position Verification:** Verification of patient positioning is a vital process for efficient outcomes in radiation therapy. Currently electronic portal images are used for patient position evaluation. This is achieved after direct comparison with the DRRs. This approach based on 2D methods and thus it can be hard to control the position variations. New techniques are currently under development, which employ the use of 3D imaging directly in the treatment room. For this technique to get established volume visualization and registration techniques have to be investigated and proposed.

# References

---

- [AcqSim] <http://www.medical.philips.com/main/products/ros/products/Acqsim/>
- [Agost01] S. Agostinelli, and F. Foppiano; **A Prototype 3D CT extension for radiotherapy simulators**, Computerized Medical Imaging and Graphic, Vol: 25, pp:11-21, 2001
- [Alast01] H. Alast, M.P. Petric, C.N. Catton, and P.R. Warde; **Portal Imaging For Evaluation Of Daily On-Line Setup Errors And Off-Line Organ Motion During Conformal Irradiation Of Carcinoma Of The Prostate**, Radiation Oncology Biol.Phys., Vol: 49, pp:869-884, 2001
- [Ament98] N. Amenta, M. Bern, and M. Kamvysselis; **A New Voronoi-Based Surface Reconstruction Algorithm**, Computer Graphics, SIGGRAPH' 1998, pp: 415-421, 1998
- [AMERSH] <http://www.amershamhealth.com>
- [Aruga00] T. Aruga, J. Itami, M. Aruga, K. Nakajima et al.; **Target Volume Definition For Upper Abdominal Irradiation Using CT Scans Obtained During Inhale And Exhale Phases**, Int. J. Radiation Oncology Biol. Phys., Vol: 48, pp:465-469, 2000
- [Atari95] N. Atari, R. Zwicker, and R. Schmidt-Ullrich; . **Performance evaluation of a prototype high resolution digital radiographic near real-time fluoroscopic computerized tomographic system for radiotherapy simulation**, Int. J. Radiation Oncology Biol. Phys., Vol: 32, pp:421-436, 1995
- [Bajaj95] C. Bajaj, F. Bernardini, and G. Xu; **Automatic Reconstruction of Surfaces and Scalar Field from 3D Scans**, Computer Graphics, SIGGRAPH' 1995, pp: 109-118, 1995
- [Balta93] D. Baltas, K.M. Sievers, and B. Kober; **Preliminary results of a intercomparison of quality control referring to therapy simulators**, ESTRO, Second Biennial Meeting on Physics in Clinical Radiotherapy. Prague 1993
- [Bedfo98] J.L. Bedford, and G.S. Shentall; **A Digital Method for Computing Target Margins in Radiotherapy**, Med.Physics, Vol: 25, pp:224-231, 1998
- [Behr00] J. Behr, S.M. Choi, S. Großkopf, H. Hong, S.A. Nam, Y. Peng, A. Hildebrand, M.H. Kim, and G. Sakas; **Modeling, Visualization, and Interaction Techniques for Diagnosis and Treatment Planning in Cardiology**, Computer & Graphics, Vol: 24, pp: 741-753, 2000
- [Beier98] J. Beier, R.C. Bittner, N. Hosten, J. Troger, and R. Felix; **Morphological Image Processing Operators: reduction of partial volume effects to improve 3D visualization based on CT data**, Radiologie, Vol: 38, pp:860-866, 1998

- [Bel93] A. Bel, M.van Herk, H. Bartelink, and J.V. Lebesque; **A Verification Procedure to Improve Patient Set-up Accuracy Using Portal Images**, Radiother. Oncol., Vol: 29, pp:253-260, 1993
- [Belsh97] R. Belshi, D. Pontvert, J.C. Rosenwald, and G. Gaboriaud; **Automatic Three-dimensional Expansion of Structures Applied to Determination of the Clinical Target Volume in Conformal Radiotherapy**, Int. J. Radiation Oncology Biol. Phys., Vol: 37, pp:689-696, 1997
- [Bergm95] L.D. Bergman, B.E. Rogowitz, and L.A. Treinish; **A Rule-based Tool for Assisting Colormap Selection**, In Proceedings of 5<sup>th</sup> IEEE Visualization Conference, pp:118-124, 1995
- [Beyer00] T. Beyer, D.W. Townsend, T. Brun, et al; **A Combined PET/CT scanner for Clinical oncology**, Journal of Nuclear Medicine, Vol: 41, pp: 1369-1379, 2000
- [Bhale00] A. Bhalariao, H. Pfister, M. Halle, and R. Kikinis; **Fast Re-Rendering Of Volume And Surface Graphics By Depth, Colour and Opacity Buffering**, Medical Image Analysis, Vol:4, pp:235-251, 2000
- [Blake98] A. Blake, and M. Isard; **Active Contours: The Application of Techniques from Graphics, Vision, Control Theory and Statistics to Visual Tracking of Shapes in Motion**. Springer-Verlag, London, 1998
- [Boer01] J.C.J. de Boer, and B.J.M. Heijmen ; **A Protocol for the Reduction of Systematic Patient Setup Errors with Minimal Portal Imaging Workload**, Int.J. Radiation Oncology Biol. Phys, Vol: 50, pp: 1350-1365, 2001
- [Boer02] J.C.J. de Boer, and B.J.M. Heijmen ; **A New Approach to Off-Line Setup Corrections: Combining Safety with Minimum Workload**, Medical Physics, Vol: 29, pp: 1998-2012, 2002
- [Boiss88] J. Boissonat; **Shape Reconstruction from Planar Cross Sections**, Computer Vision, Graphics and Image Processing, Vol: 44, pp:1-29, 1988
- [Bolle03] M.A. Bollet, H.A. McNair, V.N. Hansen et al; **Can Digitally Reconstructed Radiographs (DRRs) Replace Simulation Films in Prostate Cancer Conformal Radiotherapy?**, Int. J. Radiation Oncology Biol. Phys., Vol: 57, pp:1122-1130, 2003
- [Books89] F. L. Bookstein, **Principal Warps: Thin Plate Splines and the Decomposition of Deformations**, IEEE Transactions on Pattern Analysis and Machine Intelligence, Vol: 11, pp:567-585, 1989
- [Brown97] M.S. Brown, M.F. McNitt-Gray, N.J. Mankovich, J.G. Goldin, J. Hiller, and L.S. Wilson D.R. Aberle; **Method for Segmenting Chest CT Image Data Using an Anatomical Model: Preliminary Results**, IEEE Trans. On Medical Imaging, Vol: 16, pp: 828-839, 1997
- [Butke96] E.K. Butker, D.J. Helton, J.W. Keller, L.L. Hughes, T. Crenshaw, and L.W. Davis; **A Totally Integrated Simulation Technique for Three Field Breast Treatment Using a CT Simulator**, Med. Phys., Vol: 23, pp: 1809-1814,1996

- [CaiJ99] J. Cai, J.C. Chu, D. Recine et al; ***CT and PET lung Image Registration and Fusion in Radiotherapy Treatment Planning Using the Chamfer-Matching Method***, Int. J. Radiation Oncology Biol. Phys., Vol: 43, pp:883-891, 1999
- [Cai98] W. Cai, and G. Sakas; ***Maximum intensity projection using splatting in sheared object space***. In Proceedings EUROGRAPHICS '98, pp: 113-124, 1998
- [Cai99] W. Cai; ***Transfer functions in DRR volume rendering***, In Proceedings of Computer Assisted Radiology and Surgery, CARS'99, Paris, France, 1999
- [CaiSa99] W. Cai, and G. Sakas; ***Data Intermixing and Multi-Volume Rendering***, In Proceedings of Eurographics'99, Vol:18, 1999
- [Caldw03] C.B. Caldwell, K. Mah, M. Skinner et al; ***Can PET Provide the Extend of Tumor Motion for Individualized Internal Target Volumes? A Phantom Study of The Limitations of CT and Promise of PET***, Int. J. Radiation Oncology Biol. Phys., Vol: 55, pp: 1381-1393, 2003
- [Carr01] J.C. Carr, T.J. Mitchell, R.K. Beatson, J.B. Cherrie, W.R. Fright, B.C. McCallumm and T.R. Evans; ***Reconstruction and representation of 3D Objects with Radial Basis Functions***, Computer Graphics, SIGGRAPH' 2001, pp: 67-76, 2001
- [Carr97] J.C. Carr, W.R. Fright, and R.K. Beatson; ***Surface Interpolation with Radial Basis Functions for Medical Imaging***, ' IEEE Trans. Medical Imaging, Vol: 16, pp:96-107, 1997
- [Carr98] J.C. Carr, A.H. Gee, R.W. Prager, and K.J. Dalton; ***Quantitative Visualization Of Surfaces From Volumetric Data***, Proceedings Of WSGC'98 - The Sixth International Conference In Central Europe On Computer Graphics And Visualization, Pilzen, Czech Republic, Vol:1, pp:57-64, 1998
- [Castr98] S. Castro, A. König, H. Löffelmann, E. Gröller; ***Transfer Function Specification For The Visualization Of Medical Data***, Technical Report TR-186-2-98-12, Institute of Computer Graphics and Algorithms, Vienna University of Technology, 1998
- [Cehri91] M.A. Cehring, T.R. Mackie, S.S. Kubsad, B.R. Paliwal, M.P. Mehta, and T.J. Kinsella; ***A Three-Dimensional Volume Visualization Package Applied To Stereotactic Radiosurgery Treatment Planning***, Int. J. Radiation Oncology Biol. Phys., Vol:21, pp:491 -500, 1991
- [Chala97] V. Chalana, Y. Kim; ***A Methodology for Evaluation of Boundary Detection Algorithms on Medical Images***, IEEE Trans.On Medical Imaging, Vol:16, pp:642-652, 1997
- [Chee99] C. Chee-Wai, and D.J. Indra; ***Treatment Plan Evaluation Using Dose-Volume Histogram (DVH) and Spatial Dose-Volume Histogram (zDVH)***, Int. J. Radiation Oncology Biol. Phys., Vol: 43, pp:1143-1150, 1999
- [Chen96] G.T.Y. Chen, C.A. Pelizzari, and S. Vijayakumar; ***Imaging: The Basis for Effective Therapy***, Front Radiat Ther Oncol, Vol: 29, pp:31-42, 1996

- [Cho98] P. S. Cho, K. L. Lindsley, J. G. Douglas, K. J. Stelzer, and T. W. Griffin; ***Digital Radiotherapy Simulator***, Computerized Medical Imaging and Graphic, Vol: 22, pp:1-7, 1998
- [Cohen01] E. Cohen, R.F. Riesenfeld, and G. Elber; ***Geometric Modeling with Splines: An Introduction***, A.K. Peters Ltd, 2001
- [Conw97] J. Conway, and M.H. Robinson; ***CT Virtual Simulation***, British Journal of Radiology, Vol: 70, pp:106-118, 1997
- [Crawf96] C. Crawford, K. King, C. Ritchie, and D. Dodwin; ***Respiratory Compensation in Projection Imaging Using a Magnification and Displacement Model***, IEEE Trans. On Medical Imaging, Vol: 15, pp: 327-332, 1996
- [Culli93] T.J. Cullip, J.R. Symon, J.G. Rosenman, and E.L. Chaney; ***Digitally Reconstructed Fluoroscopy And Other Interactive Volume Visualizations In 3-D Treatment Planning***, Int. J. Radiation Oncology Biol. Phys., Vol:27, pp:145-151, 1993
- [DasCh98] I.J. Das, E.C. Cheng, G. Freedman, and B. Fowble; ***Lung And Heart Volume Analyses With CT Simulator In Radiation Treatment Of Breast Cancer***, Int. J. Radiation Oncology Biol. Phys., Vol:42, pp:11-19, 1998
- [Dawso98] L.A. Dawson, K. Mah, E. Franssen, and G. Morton; ***Target Position Variability Throughout Prostate Radiotherapy***, Int. J. Radiation Oncology Biol. Phys., Vol: 42, pp:1155-1161, 1998
- [Dehm99] J. Dehmeshki; ***An Adaptive Segmentation and 3-D Visualisation of the Lungs***, Pattern Recognition Letters, Vol: 20, pp:919-926, 1999
- [Desbr99] M. Desbrun, M. Meyer, P. Schröder, and A.H. Barr; ***Implicit Fairing Of Irregular Meshes Using Diffusion And Curvature Flow***, Computer Graphics, SIGGRAPH' 99, pp: 317-324, 1999
- [Dicks03] S. Dickson, G. Lawrence, D. Parr, and G. Lambert; ***CT Simulation in a Large Department Using SOMATOM Emotion Duo Scanner***, Electromedica, Vol: 71, pp:28-35, 2003
- [Donov00] E. Donovan, U. Johnson, G. Shentali, P.M. Evans, A.J. Neal, and J.R. Yarnold; ***Evaluation Of Compensation In Breast Radiotherapy: A Planning Study Using Multiple Static Fields***, Radiation Oncology Biol.Phys, Vol: 46, pp:671-679, 2000.
- [Drebi88] R.A. Drebin, L. Carpenter, and P. Hanrahan; ***Volume Rendering***, Computer Graphics, SIGGRAPH 1988, pp: 65-74, 1988
- [Drzym91] R.E. Drzymala, R. Mohan, L. Brewster, J. Chu, M. Goitein, W. Harms, and M. Urie; ***Dose-Volume Histograms***, Int. J. Radiation Oncology Biol. Phys., Vol: 21, pp: 71-78, 1991
- [EdWon02] G. K. Edmundson, J. Wong, D. Yan, D. Lockman, D. Brabbins *et al.*; ***Adaptive Radiation Therapy [ART] for Prostate Cancer at William Beaumont Hospital***, In Progress in CT-3D Simulation, 1st Exomio User Meeting, Lemesos-Cyprus, November, 2002

- [Encar96] J. L. Encarnaç o, W. Stra er, R. Klein; **Graphische Datenverarbeitung II. Modellierung komplexer Objekte und photorealistische Bilderzeugung** In: Oldenbourg Verlag, ISBN 3-486-23469-2, 1996
- [Encar01] J. L. Encarnaç o, In: Earnshaw, Rae A. et al.; **Challenges and Frontiers of Computer Graphics: A Vision for an Applied Research Agenda**, Frontiers of Human-Centred Computing, Online Communities and Virtual Environments, London, Berlin, Heidelberg: Springer-Verlag, pp: 367–393, 2001
- [Encar03] J. L. Encarnaç o and P. Blachetta; **Entwicklung der Graphischen Datenverarbeitung seit 1975**, Die Darmst dter, deutsche und europ ische Sicht - insbesondere gesehen durch die Printmedien Darmstadt: INI- GraphicsNet-Stiftung, 2003
- [Exomio] <http://www.igd.fhg.de/www/igd-a7/pro/Exomio/EXOMIO.html>
- [Elbak02] A. Elbakri, and J.A. Fessler; **Statistical Image Reconstruction for Polyenergetic X-Ray Computed Tomography**, IEEE Trans. Medical Imaging, Vol: 21, pp: 89-99, 2002
- [FangB98] S. Fang, T. Biddlecome, and M. Tuceryan; **Image-Based Transfer Function For Data Exploration In Volume Visualization**, In Proceedings of IEEE Visualization'98, pp: 319-316, 1998
- [FocalS] <http://www.cms-stl.com/>
- [Fraas98] B.A. Fraass, K.L. Lash, G.M. Matrone et al.; **The Impact of Treatment Complexity and Computer-Control delivery Technology on Treatment Delivery Errors**, Int.J. Radiation Oncology Biol.Phys., Vol: 42, pp:651-659, 1998
- [Galvi95] J.M. Galvin, C. Sims, G. Dominiak, and J. Cooper; **The Use Of Digitally Reconstructed Radiographs For Three-Dimensional Treatment Planning And CT-Simulation**, Radiation Oncology Biol.Phys, Vol: 31, pp: 935-942F, 1995
- [GE] <http://www.ge.com>
- [Gehri91] M.A. Gehring, T.R. Mackie, S.S. Kubsad, B.R. Paliwal, M.P. Mehta, and T.J. Kinsella; **A Three-Dimensional Volume Visualization Package Applied To Stereotactic Radiosurgery Treatment Planning**, Radiation Oncology Biol.Phys, Vol: 21, pp: 491-500, 1991
- [Geets04] X. Geets, J-F. Daisne, V. Gregoire, M. Hamoir, and M. Lonneux; **Role of 11-C-Methionine Positron Emission Tomography for the Delineation of the Tumor Volume in Pharyngo-Laryngeal Squamous Cell Carcinoma: Comparison with FDG-PET and CT**, Radiotherapy & Oncology, Vol: 71, pp:267-273, 2004
- [Geige93] B. Geiger; **Three-dimensional modeling of human organs and its application to diagnosis and surgical planning**, PhD Thesis, Ecole des Mines de Paris, 1993
- [Gerst99] N. Gerstner, S. Wachter, T.H. Knocke, C. Fellner, A. Wambersie, and R. P tter; **The Benefit of beam's Eye View based 3D Treatment Planning for Cervical Cancer**, Radiotherapy and Oncology, Vol: 51, pp: 71-78, 1999

- [GibsM98] S. Gibson; ***Constrained Elastic Surface nets: generating smooth surfaces from binary segmented data***, In Proceedings of Medical Image Computing and Computer Assisted Interventions (MICCAI), W.M. Wells, A. Colchester, and S. Delp, eds., Lecture Notes in Computer Science 1496, Springer-Verlag, pp. 888-898, 1998
- [Gibso98] S. Gibson; ***Using Distance Maps For Accurate Surface Representation In Sampled Volumes***, In Proceedings of the Symposium on Volume Visualization, ACM SIGGRAPH, pp. 23-30, 1998
- [Gibso97] S. Gibson, and A. Mirtich; ***A Survey of Deformable Modeling in Computer Graphics***, Technical Report TR97-19, MERL Technical Report, 1997
- [Gordo94] D. Gordon, M.A. Peterson, and R.A. Reynolds; ***Fast polygon Scan Conversion With Medical Applications***, IEEE Computer Graphics and Application, Vol: 14, pp: 20-27, 1994
- [Grees00] H. Greess, A. Nömayr, B. Tomandl, M. Blank, M. Lell, M. Lenz, and W.A. Bautz; ***2D and 3D Visualisation of Head and Neck Tumours from Spiral-CT Data***, European Journal of Radiotherapy, Vol: 33, pp: 170-177,2000
- [Gripp99] S. Gripp, R. Doeker, M. Glag, P. Vogelsang, et al.; ***The Role of CT Simulation in Whole-Brain Irradiation***, Int. J. Radiation Oncology Biol. Phys., Vol: 45, pp:1081-1088, 1999
- [Gross98] S. Grosskopf, S.Y. Park, and M.H. Kim; ***Segmentation of Ultrasonic Images by Application of Active Contour Models***, In Proceedings CARS 1998, Computer Assisted Radiology and Surgery, Tokyo, Japan, pp: 871-877, 1998
- [Gross02] S. Grosskopf, J.L. Encarnação (Referent); G. Sakas (Referent); ***Realitätsnahe Modellierung und Visualisierung dynamischer medizinischer Bilddaten mittels aktiver Konturen, aktiver Regionen und deformierbarer Modelle***, Darmstadt, Techn. Univ., Diss., 2002
- [Haral85] M. Haralick, and G. Shapiro; ***Image segmentation techniques***, Comput. Vis. Graph. Im. Proc., Vol: 29, pp: 100-132, 1985
- [HeHoK96] T. He, L. Hong, A. Kaufman, and H. Pfister; ***Generation Of Transfer Function With Stochastic Search Techniques***, In Proceedings of IEEE Visualization, 1996
- [Herma01] M.G. Herman, J.M. Balter, D.A. Jaffray et al.; ***Clinical use of Electronic Portal Imaging: Report of AAPM Radiation Therapy Committee Task Group 58***, Medical Physics, Vol: 28, pp:712-737, 2001
- [Heusc99] D.J. Heuscser, M. Vembar; ***Reduced Partial Volume Artifacts using Computed Tomography and an Interpolator***, Medical Physics, Vol: 26, pp:276-286, 1999
- [Höhne90] K.H. Höhne, M. Bomans, A. Pommert, et al.; ***3D Visualization Of Tomographic Volume Data Using The Generalized Voxel Model***, The Visual Computer, Vol:6, pp:28-36, 1990

- [Hoppe92] H. Hoppe, T. DeRose, T. Duchamp, J. McDonald, and W. Stuetzle; **Surface Reconstruction from Unorganised Points**, Computer Graphics, SIGGRAPH' 1992, pp: 71-78, 1992
- [Houst02] M. Houston, A. Gribbin, and M. Maher; **Virtual Simulation: Breast, Pelvic and Head & Neck Cancers**, In Progress in CT-3D Simulation, 1st Exomio User Meeting, Lemessos-Cyprus, November, 2002
- [Hu01] S. Hu, E.A. Hoffman, and J.M. Reinhardt; **Automatic Lung Segmentation for Accurate Quantitation of Volumetric X-Ray CT Images**, IEEE Trans. On Medical Imaging, Vol: 20, pp:490-498, 2001
- [Humm95] J.L. Humm, D. Pizzuto, E. Fleischman, and R. Mohan; **Collision Detection and Avoidance During Treatment Planning**, Int. J. Radiation Oncology Biol. Phys., Vol: 33, pp:1101-1108, 1995
- [Hurkm01] C.W. Hurkmans, J.H. Borger, B.R. Pieters, N.S. Russell, E.P.M. Jansen, and B.J. Mijnheer; **Variability in Target Volume Delineation on CT Scans of the Breast**, Int. J. Radiation Oncology Biol. Phys., Vol: 50, pp:1366-1372, 2001
- [Kalen01] W.A. Kalender; **Computed Tomography: Fundamentals, System Technology, Image Quality, Applications**, Wiley & Sons, New York, 2001
- [Kalet97] I.J. Kalet; **Designing Radiotherapy Software Components and Systems that will work together**, Seminars in Radiation Oncology, Vol: 7, pp:11-20, 1997
- [Karan01] G. Karangelis, N. Zamboglou, G. Sakas, and D. Baltas; **EXOMIO: A 3D Simulator for External Beam Radiotherapy**, International Workshop on Volume Graphics, Stony Brook, New York, 2001
- [Karan02] G. Karangelis, N. Zamboglou; **Evaluation of Patient Treatment Setup in Exomio Using Digital Portal Images**, In Progress in CT-3D Simulation, 1st Exomio User Meeting, Lemessos-Cyprus, November, 2002
- [Kass87] M. Kass, A. Witkin, and D. Terzopoulos; **Snakes: Active Contour Models**, IEEE First Int. Conf. Comput. Vision, pp: 259-268, 1987
- [Kessl94] M.L. Kessler, R.K. Ten Haken, B.A. Fraass, and D.L. McShan; **Expanding the Use and Effectiveness of Dose-Volume Histograms for 3D Treatment Planning. I: Integration of 3D Dose-Display**. Int. J. Radiation Oncology Biol. Phys., Vol: 29, pp:1125-1131, 1994
- [Kessl95] M.L. Kessler, D.L. McShan, and B.A. Fraass; **A Computer-Controlled Conformal Radiotherapy System. III: Graphical Simulation And Monitoring Of Treatment Delivery**, Radiation Oncology Biol. Phys, Vol: 33, pp:1173-1180, 1995
- [Ketti97] C.H. Ketting, M.A. Seymour, I. Kalet et al.; **Automated Planning Target Volume Generation: An Evaluation Pitting A Computer-Based Tool Against Human Experts**, Int. J. Radiation Oncology Biol. Phys., Vol: 37, pp:697-704, 1997

- [Khoo97] V.S. Khoo, D.P. Dearnaley, and Finnigan D.J.; ***Magnetic Resonance Imaging (MRI): Considerations and Applications in Radiotherapy Treatment Planning***; Radiotherapy and Oncology, Vol:42, pp:1-15, 1997
- [Khoo98] V.S. Khoo, J.L. Bedford, S. Webb, and D.P. Dearnaley; ***Comparison of 2D and 3D Algorithms for Adding a Margin to the Gross Tumor Volume in the Conformal Radiotherapy Planning of Prostate Cancer***; Int. J. Radiation Oncology Biol. Phys., Vol: 42, pp:673-679, 1998
- [Killo01] H.J. Killoran, H.E. Baldini, J.C. Beard, and L. Chin; ***A Technique for Optimization of Digitally Reconstructed Radiographs of the Chest in Virtual Simulation***, Int. J. Radiation Oncology Biol. Phys., Vol:49, pp:231-239, 2001
- [Kobbe98] L. Kobbelt, S. Campagna, J. Vorsatz, and H.P. Seidel; ***Interactive Multi-Resolution Modeling on Arbitrary Meshes***, Computer Graphics, SIGGRAPH'98, pp: 105-114, 1998
- [Kolot99] C. Kolotas, D. Baltas, and N. Zamboglou; ***CT-Based interstitial HDR brachytherapy***, Strahlenther Onkol., Vol: 175, pp: 419-27, 1999
- [Kuszy95] B.S. Kuszyk, D.R. Ney, and E.K. Fishman; ***The Current State of the Art in Three Dimensional Oncologic Imaging: An Overview***, Int. J. Radiation Oncology Biol. Phys., Vol:33, pp:1029-1039, 1995
- [Kwa98] S.L. Kwa, J.C. Theuws, and M. Van Herk; ***Automatic three-dimensional Matching of CT-SPECT and CT-CT to Localize Lung Damage After Radiotherapy***, J. of Nuclear Medicine, Vol: 39, pp:1074-1080, 1998
- [Lange01] K. Langen, and D. Jones; ***Organ Motion and its Management***, Int. J. Radiation Oncology Biol. Phys., Vol: 50, pp: 265-278, 2001
- [Laure94] P.J. Laurent, A.Le Mehaute, and L.L. Schumaker; ***Curves and Surfaces in Geometric Design***, A.K. Peters Ltd, 1994
- [Lee97] S. Lee, G. Wolberg, and S.Y. Shin; ***Scattered Data Interpolation With Multi-level B-Splines***, IEEE Transactions On Visualization And Computer Graphics, Vol:3, pp:228-244, 1997
- [Lee99] J.S. Lee, A.B. Jani, C.A. Pelizzari et al.; ***Volumetric Visualization Of Head And Neck CT Data For Treatment Planning***, Int. J. Radiation Oncology Biol. Phys., Vol:44, pp:693-703, 1999
- [LeFuP90] M. Levoy, H. Fuchs, S.M. Pizer, et al.; ***Volume Rendering In Radiation Treatment Planning***, First Conference On Visualization In Biomedical Computing, pp:4-10, 1990
- [LevoA90] M. Levoy; ***Efficient Ray Tracing Of Volume Data***, ACM Transactions On Graphics, Vol: 9, pp:245-261,1990
- [LevoB90] M. Levoy; ***Volume Rendering By Adaptive Refinement***, The Visual Computer, Vol: 6, pp:2-7, 1990
- [Levoy88] M. Levoy; ***Display of Surface from Volume Ddata***, IEEE Computer Graphics & Applications, Vol: 8, pp:29-37, 1988

- [Levoy90] M. Levoy; **A Hybrid Ray For Rendering Polygon and Volume Data**, IEEE Computer Graphics And Applications, Vol:10, pp:33-40, 1990
- [Lien84] S. Lien, and T. Kajiyu; **A Symbolic Method For Calculating The Integral Properties Of Arbitrary Nonconvex Polyhedra**, IEEE Computer Graphics And Applications, Vol:4, 1984.
- [Liu01] X. Liu, H. Bao, P. Heng, T.T. Wong, and Q. Peng; **Constrained Fairing for Meshes**, Computer Graphics, Vol: 20, pp:115-123, 2001
- [Loren87] W. Lorenson, and E.C. Harvey; **Marching Cubes: A High Resolution 3-D Surface Construction Algorithm**, Computer Graphics, SIGGRAPH'87, pp: 163-169, 1987
- [LuH99] H.M. Lu, and L. Chin; **Virtual Light Field Projection for CT-Simulation**, Med. Phys., Vol: 26, pp:1222-1229, 1999
- [LuY95] Y. Lu, S. Li, D. Spelbring, P. Song, S. Vijayakumar, C. Pelizzari, and G. Chen; **Dose-surface histograms as a treatment planning tool for prostate conformal therapy**, Med. Phys., Vol: 22, pp:279-284, 1995
- [Maise02] M.N. Maisey; **Overview of Clinical PET**, British Journal of Radiology, Vol: 75, pp: 1-5, 2002
- [McIne96] T. McInerney, and D. Terzopoulos; **Deformable Models in Medical Image Analysis: A Survey**, Medical Image Analysis, Vol: 1, pp: 91-108, 1996
- [Masut96] Y. Masutani, K. Masamune, and T. Dohi; **Region-Growing based Feature Extraction Algorithm for Tree-like Objects**, In Lecture Notes in Computer Science, K.H. Höhne and R.Kikinis Berlin, Germany :Springer Verlag, Vol: 1131, pp:161-171, 1996
- [Max95] N. Max; **Optical Models For Direct Volume Rendering**, IEEE Transactions On Visualization And Computer Graphics, Vol: 1, pp:99-108, 1995
- [McJur01] M. McJury, P.M. Fisher, S. Pledge et al.; **The Impact of Virtual Simulation in Palliative Radiotherapy for non-small-cell Lung Cancer**, Radiotherapy and Oncology, Vol: 59, pp:311-318, 2001
- [Mcken00] A.L. McKenzie, M.V. Herk, and B. Mijnheer; **The Width of Margins in Radiotherapy Treatment Plans**, Phys.Med.Biol., Vol: 45, pp:3331-3342, 2000
- [Meyer92] D. Meyers, S. Skinner, and K. Sloan; **Surfaces from contours**, ACM Transactions On Graphics, Vol: 11, pp: 228-258, 1992
- [Meyer96] J.L. Meyers, J.S. Purdy; **3D Conformal Radiotherapy**, Frontiers in Radiotherapy and Oncology, Basel, Vol: 29, 1996
- [Micha96] J.M. Michalski, J.A. Purdy, W. Harms, and J.W. Matthews; **The CT-Simulation 3D Treatment Planning Process**, Front Radiat Ther Oncol, Vol: 29, pp:43-56, 1996
- [Mihaj99] Z. Mihajlovic, and A. Coluban; **The B-Spine Interpolation in Visualization**, Journal of Computing and Information – CIT 7, Vol:3, pp:245-253, 1999
- [Mock99] U. Mock, K. Dieckmann, U. Wolff, T.H. Knocke, and R. Pötter; **Portal Imaging Based Definition Of The Planning Target Volume During Pelvic Irra-**

- diation For Gynecological Malignancies*, Radiation Oncology Biol.Phys, Vol: 45, pp:227-232, 1999
- [Möller97] T. Möller, R. Machiraju, K. Mueller, and R. Yagel; ***Evaluation And Design Of Filters Using A Taylor Series Expansion***, IEEE Transactions On Visualization And Computer Graphics Vol: 3, pp:184-199, 1997
- [Morse01] B.S. Morse, T.S. Yoo, P. Rheingans, D.T. Chen, and K.R. Subramanian; ***Interpolating Implicit Surfaces from Scattered Surface Data Using Compactly Supported Radial Basis Functions***, In Proceedings of International Conference on Shape Modelling and Applications. IEEE Computer Society Press, pp: 89-98, 2001
- [MorzK00] L. Mroz, A. König, and E. Gröller; ***Maximum intensity projection at warp speed***, *Computers & Graphics*, Vol: 24, pp: 343-352, 2000
- [MorzH00] L. Mroz, H. Hauser, and E. Gröller; ***Interactive high-quality maximum intensity projection***, In Proceedings of EUROGRAPHICS' 00, pp: 341-350, 2000
- [Nagat90] Y. Nagata, T. Nishidai, M. Abe, et al.; ***CT Simulator: A New 3-D Planning and Simulating System for Radiotherapy: Part 2. Clinical Application***, Int. J. Radiation Oncology Biol. Phys., Vol: 18, pp:505-513, 1990
- [Niels93] G.M. Nielson; ***Scattered Data Modeling***, IEEE Computer Graphics & Applications, Vol: 13, pp: 60-70, 1993
- [Niemi94] A. Niemierko, and M. Goitein; ***Dose volume distributions: a new approach to dose-volume histograms in three dimensional treatment planning***, Med. Phys., Vol: 21, pp:3-11, 1994
- [Nishi90] T. Nishidai, Y. Nagata, M. Takahashi, et al.; ***CT Simulator: A New 3-D Planning and Simulating System for Radiotherapy: Part 1. Description of System***, Int. J. Radiation Oncology Biol. Phys., Vol: 18, pp:499-504, 1990
- [O'Doh02] M.J. O'Doherty, E.A. Macdonald, S.F. Barrington, N.G. Mikhaeel, and S. Schey; ***PET in the Management of Lymphomas***, Clinical Oncology, Vol: 14, pp: 415-426, 2002
- [Ohtak01] Y. Ohtake, A. Belyaev, and I. Bogaevski; ***Mesh Regularization and Adaptive Smoothing***, Computer-Aided Design, Vol: 33, pp: 789-800, 2001
- [Olien93] J. Oliensis; ***Local Reproducible Smoothing Without Shrinkage***, IEEE Trans. on Pattern Analysis and Machine Intelligence, Vol: 15, pp: 307-312, 1993
- [Pavlid90] T. Pavlidis, and Y.Tay Liow; ***Integrating Region Growing and Edge Detection***, IEEE Trans. on Pattern Analysis and Machine Intelligence, Vol: 12, pp: 225-233, 1990
- [Payne94] B.A. Payne, and A.W. Toga; ***Surface Reconstruction By Multiaxial Triangulation***, IEEE Computer Graphics and Applications, Vol: 14, pp:28-35, 1994

- [Pekar04] V. Pekar, T.R. McNutt, and M. R. Kaus; ***Automated Model-based Organ Delineation for Radiotherapy Planning in Prostatic Region***, Int. J. Radiation Oncology Biol. Phys., Vol: 60, pp:973-980, 2004
- [Peliz96] C.A. Pelizzari, R. Grzeszczuk, G.T.Y. Chen, et al.; ***Volumetric Visualization Of anatomy For Treatment Planning***, Int. J. Radiation Oncology Biol. Phys., Vol:34, pp:205 -211, 1996
- [Peliz98] C.A. Pelizzari; ***Image Processing In Stereotactic Planning: Volume Visualization and Image Registration***, Medical Dosimetry, Vol: 23, pp: 137-145, 1998
- [Perez94] C. Perez, J.A. Purdy, W. Harms, et al.; ***Design of a Fully Integrated Three-dimensional Computed Tomography Simulator and Preliminary Clinical Evaluation***, Int. J. Radiation Oncology Biol. Phys., Vol: 30, pp:887-897, 1994
- [Perez95] C.A. Perez, J.A. Purdy, W. Harms, et al.; ***Three-dimensional Treatment Planning and Conformal Radiation Therapy: Preliminary Evaluation***, Radiotherapy and Oncology, Vol: 36, pp:32-43, 1995
- [Press93] W.H. Press, B.P. Flannery, S.A. Teukolsky, and W.T. Vetterling; ***Numerical Recipes in C : The Art of Scientific Computing***, 1993.
- [Purdy93] J.A. Purdy, W.B. Harms, J.W. Matthews, et al.; ***Advances In 3-Dimensional Radiation Treatment Planning Systems: Room-View Display With Real Time Interactivity***, Radiation Oncology Biol.Phys, Vol: 27, pp:933-944, 1993
- [Purdy96] J.A. Purdy; ***3D Radiation Treatment Planning: A New Era***, Front Radiat Ther Oncol. Basel, Karger, Vol: 29, pp:1-16, 1996
- [Ragan96] D.P. Ragan, J.D. Forman, T. He, and C.F. Mesina; ***Clinical Results of Computerized Tomography-based Simulation with Laser Patient Marking***, Int.J.Radiation Oncology Biol.Phys ., Vol: 34, pp:691-695, 1996
- [Rams98] C.R. Ramsey, and A.L. Oliver; ***Magnetic Resonance Imaging based Digitally Reconstructed Radiographs, Virtual Simulation, and Three-dimensional Treatment Planning for Brain Neoplasms***, Medical Physics, Vol: 25, pp: 1928-1934, 1998
- [Ritch96] C. Ritchie, C. Crawford, D. Godwin, K. King, and Y. Kim; ***Correction of Computer Tomography Motion Artifacts Using Pixel-Specific Back-Projection***, IEEE Trans.On Medical Imaging, Vol: 15, pp:333-342, 1996
- [RitmA80] E. Ritman; ***Physical and Technical Considerations in the Design of the DSR, and High Temporal Resolution Volume Scanner***, American Journal of Roentgenology, Vol: 134, pp: 369-374, 1990
- [RitmB90] E. Ritman; ***Fast Computed Tomography for Quantitative Cardiac Analysis-State of the Art and Future Perspectives***, Mayo Clin Proceedings, Vol: 65, pp:2724-2727, 1990
- [Rohli99] R. Rohling, A. Gee, and L. Berman; ***A Comparison of Freehand Three-dimensional Ultrasound Reconstruction Techniques***, Medical Image Analysis, Vol: 3, pp:339-359, 1999

- [Rose96] J. Rosenman; ***Where Will 3D Conformal Radiation Therapy Be at the End of the Decade?***, Front Radiation Therapy Oncology, Vol: 29, pp:264-271, 1996
- [Rosen91] J. Rosenman, S. Sailer, G. Sherouse, E.L. Chaney, and J.E. Tepper; ***Virtual Simulation: Initial Clinical Results***, Int. J. Radiation Oncology Biol. Phys., Vol: 20, pp:843-851, 1991
- [Sabel88] P. Sabela; ***A Rendering Algorithms for Visualizing 3D Scalar Fields***, Computer Graphics, SIGGRAPH' 88, pp: 51-58, 1988
- [Sakas93] G. Sakas; ***Interactive Volume Rendering of Large Fields***, The Visual Computer, Vol: 9, pp:425-438, 1993
- [Sakas95] G. Sakas, M. Grimm, and A. Savopoulos; ***Optimised maximum intensity projection (MIP)***, Rendering Techniques'95, Springer Verlag, pp:51-63, 1995
- [Sakas01] G. Sakas, G. Karangelis, and A. Pommert; ***Advanced Applications of Volume Visualization Methods in Medicine***. In Advanced Signal Processing Handbook, Theory and Implementation for Radar, Sonar, and Medical Imaging Real-Time Systems, Edited by Stergios Stergiopoulos, CRC Press, ISBN 0-8493-3691-0, 2001
- [SanGa95] P. Santiago, and H.D. Gage; ***Statistical-models of Partial Volume Effect***, IEEE Trans. On Image Processing, Vol: 4, pp.1531-1540, 1995
- [Sato00] Y. Sato, C. Westin, A. Bhalerao, S. Nakajima, N. Shiraga, T. Tamura, and R. Kikinis; ***Tissue Classification Based On 3D Local Intensity Structures for Volume Rendering***, IEEE Trans. On Visualization and Computer Graphics, Vol: 6, pp.160-179, 2000
- [Savch95] V. Savchenko, A. Pasko, O. Okunev, and T. Kunii; ***Function Representation of Solids Reconstructed from Scatter Surface Points and Contours***, Computer Graphics Forum, Vol: 14, pp181-188, 1995
- [Schie00] M. Schiebe, and W. Hoffmann; ***CT-Based Virtual Simulation Using the Advantage Sim 4.1. System***, Strahlenther Onkol, Vol: 8, pp:377-380, 2000
- [Schim93] T. Schiemann, B. Dippold, R. Schmidt, et al.; ***3D Visualization For Radiotherapy Treatment Planning***, In Proceedings of Computer Assisted Radiology and Surgery, CARS '93 (H.U. Lemke, M.L. Rhodes, C.C. Jaffe, and R. Felix, eds.), Springer-Verlag, Berlin, pp:669-675, 1993
- [Seem01] M.D. Seemann, and C.D. Claussen; ***Hybrid 3D Visualization of the Chest and Virtual Endoscopy of the Tracheobronchial System: Possibilities and Limitations of Clinical Application***, Lung Cancer, Vol: 32, pp:237-246, 2001
- [Seymo95] M.A. Seymour, I. Kalet, J. McDonald, et al.; ***Three Dimensional Planning Target Volumes: A Model And A Software Tool***, Radiation Oncology Biol.Phys, Vol: 33, pp:1073-1080, 1995
- [Shale95] S. Shalev; ***Treatment Verification Using Digital Imaging***, Radiation Therapy Physics ed.AR Smith.Springer, pp:155-173, Berlin1995

- [Shero87] G. Sherouse, C. Mosher, K. Novins, J. Rosemann, and E.L. Chaney; ***Virtual Simulation: Concept and Implementation***, Proceedings of 9<sup>th</sup> International Conference of the Use of Computers in Radiation Therapy (ICCR), pp:433-436, 1987
- [Shero90] G.W. Sherouse, J.D. Bourland, K. Reynolds, H.L. McMurry, T.P. Mitchell, and E.L. Chaney; ***Virtual Simulation in the Clinical Setting: Some Practical Considerations***, Int. J. Radiation Oncology Biol. Phys., Vol: 19, pp:1059-1065, 1990
- [Shero91] G. Sherouse, and E.L. Chaney; ***The Portable Virtual Simulator***, Int. J. Radiation Oncology Biol. Phys., Vol: 21, pp:475-482, 1991
- [Shiyi01] H. Shiyang, E.A. Hoffman, and J.M. Reinhardt; ***Automatic Lung Segmentation For Accurate Quantitation Of Volumetric X-Ray CT Images***, IEEE Transactions On Medical Imaging, Vol: 20, pp:490-498, 2001
- [Siada01] M.R. Siadat, and H. Soltanian-Zadeh; ***Partial Volume Estimation using Continuous Representations***, SPIE Proc., Vol: 4322, pp:1025-1034, 2001
- [SmartS] <http://www.medical.philips.com/main/products/ros/products/smartsim/>
- [Smith90] B. Smith; ***Cone-beam tomography: recent advances and a tutorial review***, Opt. Eng., Vol: 29, pp: 521-534, 1990
- [VanSo03] J.R. Van Sornsen, R.H. Schuchhard-Schipper, S. Senan, B.J. Heijmen; ***Procedures for high precision setup verification and correction of lung cancer patients using CT-simulation and digitally reconstructed radiographs (DRR)***, Int. J. Radiation Oncology Biol. Phys., Vol: 55, pp:804-810, 2003
- [Spath95] H. Spath; ***Two Dimensional Spline Interpolation Algorithms***, A.K. Peters Ltd, 1995
- [Stras04] G. Strassmann, P. Vacha, I. Braun, D. Richter, and R. Engenhardt-Cabillic; ***Methodology of Continuous Extracranial Radiosurgery for Lung Cancer Using EXOMIO 3-D CT Simulation***, Strahlentherapie und Oncologie, Vol: 180, pp:241-244, 2004
- [StraV04] G. Strassmann, P. Vacha, T. Osterhaus, A. Battmann et. al.; ***Evaluation of a Laser System for CT Software Simulation (EXOMIO) in Patients with Breast Cancer***, Strahlentherapie und Oncologie, Vol: 180, pp:597-600, 2004
- [Taubi95] G. Taubin; ***A Signal Processing Approach To Fair Surface Design***, Computer Graphics, SIGGRAPH' 95, pp: 351-358, 1995
- [Terzo88] D. Terzopoulos, and K. Fleischer; ***Deformable Models***, The Visual Computer, Vol: 4, pp: 306-331, 1988
- [Thürm01] G. Thürmer; ***Smoothing Normal Vectors On Discrete Surfaces While Preserving Slope Discontinuities***, Computer Graphics, Vol: 20, pp:103-114, 2001
- [Thürm97] G. Thürmer, and C.A. Wüthrich; ***Normal Computation For Discrete Surfaces In 3D Space***, In Proceedings of Eurographics'97, Vol: 16, 1997

- [Tsiak01] M.F. Tsiakalos, E. Schrebmann, K. Theodorou, and C. Kappas; **Graphical Treatment Simulation and Automated Collision Detection for Conformal and Stereotactic Radiotherapy Treatment Planning**, Med.Physics, Vol: 28, pp:1359-1363, 2001
- [Turk02] G. Turk, and J.F. O'Brien; **Modelling with Implicit Surfaces that Interpolate**, ACM Transaction on Graphics, Vol: 21, pp: 1-19, 2002
- [Turk99] G. Turk, and J.F. O'Brien; **Shape Transformation Using Variational Implicit Functions**, Computer Graphics, SIGGRAPH'1999, pp. 335-342, 1999
- [TurkB99] G. Turk, and J.F. O'Brien; **Variational Implicit Surfaces**, Tech Report GIT-GVU-99-15, Georgia Institute of Technology, May 1999
- [Twidd94] R. Twiddy, J. Cavallo, and S.M. Shiri; **Restorer: A Visualization Technique for Handling Missing Data**, In Proceedings of IEEE Visualization'94, pp:212-216, 1994
- [Valen03] V. Valentini, A. Piermattei, A.G. Morganti, M.A. Gambacorta, L. Azario, et al; **Virtual simulation: fifteen years later**, Rays. Vol. 28, pp:293-298, 2003
- [ValiA97] R.K. Valicenti, F.M. Waterman, B.W. Corn, and W.J. Curran; **A Prospective Randomized Study Addressing the Need for Physical Simulation following Virtual Simulation**, Int. J. Radiation Oncology Biol. Phys., Vol: 39, pp:1131-1135, 1997
- [ValiB97] R.K. Valicenti, F.M. Waterman, R.J. Croce, B. Corn; and W.J. Curran; **Efficient CT Simulation of the Four-Field Technique For Conformal Radiotherapy of Prostate Carcinoma**, Int. J. Radiation Oncology Biol. Phys., Vol:37, pp:953-957, 1997
- [VanHe94] M. VanHerk, and H.M. Kooy; **Automatic Three-Dimensional Correlation of CT-CT, CT-MRI, and CT-SPECT using Chamfer Matching**, Medical Physics, Vol: 21, pp: 1163-1178, 1994
- [Vanuy99] L. Vanuytsel, and C. Weltens; **Imaging Techniques for Radiotherapy Planning**, Oncology in Practice, Vol: 2, pp: 18-21, 1999
- [Vasil83] V.A. Vasilenko; **Spline-functions: theory, Algorithms, Programs**, Novosibirsk, Nauka Publishers, 1983
- [VDBer00] D.L. Van De Berge, M.De Ridder, and G.A. Storme; **Imaging In Radiotherapy**, European Journal Of Radiology, Vol:34, pp:41-48, 2000
- [Verel99] D. Verellen, V. Vinh-Hung, P. Bijdekerke, et al.; **Characteristics and clinical application of a treatment simulator with CT-option**, Radiotherapy And Oncology, Vol: 50, pp:355-366, 1999
- [Vijay95] S. Vijayakumar, and G.T.Y. Chen; **Implementation of Three Dimensional Conformal Radiation Therapy: Prospects, Opportunities, and Challenges**, Int. J. Radiation Oncology Biol. Phys., Vol: 33, pp:976-983, 1995
- [Vollm99] J. Vollmer, R. Mencl, and H. Müller; **Improved Laplacian Smoothing Of Noisy Surface Meshes**, In Proceedings of Eurographics'99, Vol: 18, 1999

- [Vuong00] T. Vuong, W. Parker, H.J. Patrocino, et al.; **An Alternative Mantle Irradiation Technique Using 3D CT-based Treatment Planning for Female Patients with Hodgkin's Disease**, Int.J. Radiation Oncology Biol.Phys., Vol: 47, pp: 739-748, 2000
- [Wang94] S.W. Wang, and A.E. Kaufman; **Volume-Sampled 3D Modeling**, IEEE Computer Graphics And Applications, Vol: 14, pp: 26-32, 1994
- [Weist00] D. Weinstein; **Scanline Surfacing: Building Separating Surfaces from Planar Contours**, In Proceeding of 11<sup>th</sup> IEEE Visualization'2000, 2000
- [Wells98] D.M. Wells, and J. Niederer; **A Medical Expert System Approach Using Artificial Neural Networks for Standardized Treatment Planning**, Int.J.Radiation Oncology Biol. Phys., Vol: 41, pp:173-182, 1998
- [Welte99] L. Weltens; **Imaging Techniques for Radiotherapy Planning**, Oncology in Practice, Vol: 2, pp: 18-21, 1999
- [Whita00] R. Whitaker; **Reducing Aliasing Artifacts in Iso-Surfaces of Binary Volumes**, In Volume Visualization and Graphics Symposium 2000. ACM SIGGRAPH, pp:23-32, 2000
- [Willn03] J. Willner, A. Jost, K. Baier, and M. Flentje; **A Little to a Lot or a Lot to a Little?**, Strahlentherapie und Oncologie, Vol: 179, pp:548-556, 2003
- [Wolbe90] G. Wolberg; **Digital Image Warping**, Wiley-IEEE Press, 1st Edition, 1990
- [Wong99] J.W. Wong, M.B. Sharpe, D.A. Jaffray, et al.; **The Use of Active Breathing Control (ABC) to Reduce Margin for Breathing Motion**, Int. J. Radiation Oncology Biol. Phys., Vol: 44, pp: 911-919, 1999
- [Yan00] C.H. Yan, R.T. Whalen, G.S. Beaupre, S.Y. Yen, and S. Napel; **Reconstruction Algorithm for Polychromatic CT Imaging: Application to Beam Hardening Correction**, IEEE Trans. On Medical Imaging, Vol: 19, pp:1-11, 2000
- [Yan97] D. Yan, J. Wong, F. Vicini, J. Mchalski, C. Pan, A. Frazier, E. Horwitz, and A. Martinez; **Adaptive Modification of Treatment Planning to Minimize the Deleterious Effects of Treatment Setup Errors**, Int.J.Radiation Oncology Biol.Phys, Vol: 38, pp:197-206, 1997
- [Yoo01] T. Yoo, B. Morse, K.R. Subramanian, P. Rheingans, and M. Ackerman; **Anatomic Modeling From Unstructured Samples Using Variational Implicit Surfaces**, In Medicine Meets Virtual Reality, 2001
- [Zambo94] N. Zamboglou, T. Schnabel, C. Kolotas, W. Achterrath, H. Strehl *et al*; **Carboplatin and radiotherapy in the treatment of head and neck cancer: six years' experience**. Semin Oncol. Vol: 21, pp:45-53, 1994
- [Zambo02] N. Zamboglou, G. Karangelis, I. Nomikos, S. Zimeras, T.Helfmann *et al*; **EXOMIO Virtual Simulation: Oropharynx, Prostate & Breast Cancer**, In Progress in CT-3D Simulation, 1st Exomio User Meeting, Lemessos-Cyprus, November, 2002

- [Zelez97] M.P. Zeleznik; ***3D Visualization: What Does it Mean?***, XII International Conference On The Use Of Computers In Radiation Therapy (ICCR), MO University of Utah, Salt Lake City, pp:27-30, 1997
- [Zuide95] K.J. Zuiderveld; ***Visualization of Multimodal Medical Volume Data using Object-Orientated Methods***, PhD Thesis, Utrecht University, 1995